NATIONAL RADIO ASTRONOMY OBSERVATORY
Green Bank, West Virginia

ATMOSPHERIC ABSORPTION IN THE RANGE OF WAVELENGTH BETWEEN 10 CMS AND 1 MICRON

Rama C. Menon

JANURAY 1964

ATMOSPHERIC ABSORPTION IN THE RANGE OF WAVELENGTH BETWEEN 10 CMS AND 1 MICRON

Rama C. Menon

I. Introduction

The recent rapid development of receiver technology in the mm, sub-mm, and infrared part of the electromagnetic spectrum is making possible the exploitation of this part of the spectrum for astronomical observations. A thorough understanding of the absorption characteristics of the earth's atmosphere at the above wavelengths is of great importance for the effective planning of astronomical observations.

The basic theoretical work on microwave absorption by atmospheric gases was done by Van Vleck towards the end of World War II. Since then numerous theoretical and experimental investigations have been carried out. As a result we are in a position to evaluate the atmospheric absorption characteristics in the range 10 cms to 1 mm with reasonable accuracy for a certain elevation angle and given meteorological conditions. Little reliable information is available at the moment for the wavelength region between 20 microns and 1 mm.

The exploration of the infrared region had been started by extending astronomical observations at optical wavelengths to the near infrared. During the last war and later activity in the medium and far infrared region had been stimulated mainly by military applications. The available literature on this subject is very widespread. A report of Altshuler [1] gives an excellent summary of the work done up to 1961. The information is presented in the form of graphs for an immediate application to practical absorption calculations. Most of the results presented in this report for the infrared region are based on Altshuler's report.

The aim of this report is to give a review of the atmospheric models, to discuss briefly the physical processes connected with the atmospheric absorption and finally to calculate the zenith extinction for the whole wavelength region considered here for different reasonable meteorological conditions and sites of observation. The general trend of extinction with possible windows is presented. The radiation from the atmosphere can be predicted from such extinction data. By extinction is meant the combined effect of scattering and attenuation. Under good observation conditions the scattering can be neglected

as compared to absorption, at least in the far infrared and microwave region.

The terminology used in this report is explained here. The transmission of the atmosphere, when the line of sight subtends an angle z ("zenith distance") to the zenith, is given by the equation

(1) $$I(z)/I_{Incident} = p^{F(z)}.$$

$I_{Incident}$ means the radiation intensity of a remote radiation source outside the atmosphere and I(z) means the intensity of this source as measured by an observer at the surface of the earth. For $z < 80°$, $F(z) = \sec z$; for larger distances z, the rigorous air mass function has to be used. Also for $z = 0$, $F(z) = 1$. Hence p denotes the transmission coefficient of the total atmosphere at zenith. By means of equation (1), it is possible to calculate the transmission of the atmosphere for any zenith distance z if the transmission coefficient p is known.

On the other hand, p can be calculated from experimental extinction values at various zenith distances z. The values of p are presented in different forms by different authors. Sometimes the value -log p is given, which then is a positive number, since $p \leq 1$. Then the loss of the atmosphere, which is defined as (1 - p) can be obtained for small values of p using the relation

(2) $$1 - p = -\log_{10} p/0.4343.$$

Instead of the transmission very often the attenuation of the atmosphere is given, especially for the microwave and sub-mm region. The attenuation is then given in db and is related to the transmission by

(3) $$\text{zenith attenuation in db} = 10 \log \frac{1}{p} = -10 \log p.$$

This makes it convenient to compare -log p and zenith attenuation values given in db.

2. Model Atmospheres

In order to correlate the different experimental conditions and theoretical assumptions, one needs to consider the major models of atmospheres. The physical and chemical properties of the earth's atmosphere vary significantly with altitude. In all models, the vertical structure of atmosphere is considered as consisting of nearly concentric, approximately spherical shells with merging boundaries. Within these systems, the various shells are distinguished from each other by differences in definable and measurable parameters such as temperature, temperature gradient, ionization, predominant chemical processes or a combination of several of these and other factors. One of the accepted systems is due to Chapman (see ref. [2]). In this system the classification is based on dominant physical processes. Troposphere, stratosphere, mesosphere and thermosphere are based on temperature variations. Homosphere and heterosphere are based on composition, ionosphere on ionization, chemosphere depends on chemical reactions and exosphere is based on mechanism of molecular escape.

Troposphere is the region nearest the earth's surface extending to an altitude of about 12 to 14 km depending on the latitude. It has a uniform decrease of temperature with altitude. Temperature inversions happen however in this region as the weather changes. The tropopause is the upper boundary of troposphere extending up to 18 km. These are the regions in which electromagnetic radiation is mainly absorbed by water vapor and oxygen.

Even though there are several tabulations of various parameters describing model atmospheres, ARDC model atmosphere [2], revised at periodic intervals, is the most commonly used. Hogg [3], one of the early workers in this field, used the dependence of temperature and pressure on height based on the international standard atmosphere. The water vapor content was assumed to vary linearly from 10 gm/meter^3 at the earth's surface to zero at a height of 5 km. Several authors use various moisture contents, in conjunction with the atmospheric model chosen, depending on geographic location and latitude.

3. Atmospheric Constituents

One has to consider the composition of air in order to estimate the relative importance of various constituents. Air is a mechanical mixture of several gases. The mixing ratio of some gases, as referred to the total amount of gas, is constant and does not depend

on altitude, whereas the mixing ratio of other gases varies markedly with time and location, generally showing a rapid decrease in percentage with height. These atmospheric gases are all selective absorbers, that is, they absorb at some wavelengths but are transparent to others. An extraterrestrial radiation at these wavelengths of transparency passes through the atmosphere only slightly attenuated. These windows are therefore of special interest for earthbound observers.

The major constituents in the troposphere are molecular nitrogen (N_2, 78%), molecular oxygen (O_2, 21%), and argon (A, 1%). The minor constituents are carbon dioxide (CO_2), neon (Ne), helium (He), molecular hydrogen (H_2) and variable amounts of carbon monoxide (CO), methane (CH_4), nitrogen dioxide (NO_2), nitrous oxide (N_2O), water vapor (H_2O) and ozone (O_2). The predominance of these major and minor constituents and variable gases changes with altitude. Although water vapor usually comprises less than 3% of the gases even with moist conditions at sea level, it absorbs in the wavelength region considered here nearly six times as much solar radiation as do all of the other gases combined.

The following gases have approximately constant mixing ratios as referred to the total amount of air at altitudes between 0 to 50 km.

Table 1. Concentration of Infrared Absorbing Gases [1]

Gas	Concentration (parts per million)	Amount in 1 km path at sea level, atm-cm
CO_2	320	32.0
N_2O	0.27	0.027
CH_4	2.4	0.24
CO	1.1	0.11

For example, CO_2 exists in the atmosphere in the proportion of 0.032% by volume (or 320 parts by million), which means that for every km of air at sea level, the light ray traverses 32 atm-cm of CO_2. The energy transition of these atmospheric components contribute attenuation mainly in the infrared region which will be discussed in section 11.

4. Precipitable Water Vapor

It is customary to express the amount of water vapor concentration, w, in the atmosphere in precipitable cms. There are two notations, denoted by subscripts h and v depending on whether the atmosphere path considered is horizontal or vertical. w_h represents the thickness of the layer of liquid water that would be formed, if all water vapor traversed by a light beam were condensed in a container of cross sectional area equal to that of the parallel beam. The value of precipitable cm of water in a horizontal path, w_h, can be found from water vapor density and path length by an empirical formula [1] as given below.

(4) $$w_h = \rho_w x/10$$

where w_h = precipitable water content in horizontal path in cms
ρ_w = water vapor density (gms m^{-3})
x = path length in km

For the zenith attenuation calculations, the more important quantity is the vertical water vapor content of the atmosphere over a given place, in an air column of cross-sectional area of 1 cm^2. This quantity is called precipitable cm in a vertical path and is denoted by w_v. The total amount of water vapor contained between the height 0 and the height z would be

(5) $$w_v = \int_0^z \rho_w \, dz$$

Since by definition the precipitable water is referred to a column of cross section 1 cm^2, w_v can be expressed in either cms or gms/cm^2.

w_v can be expressed in different forms, depending on the data available. The hydrostatic equation in the atmosphere is

(6) $$dp = -\rho g \, dz,$$

and the equation of state for water vapor is given by

(7) $$e = \rho_w \frac{R}{m_w} T$$

where e = partial pressure of water vapor

ρ_w = water vapor density or absolute humidity

m = gm molecular weight.

The above two equations along with (5) give useful relations to obtain w_v.

Also, at saturation ρ_{ws} is given by equation (7) for corresponding saturation conditions. The values of saturation humidity at different temperatures are available [4] and these are valuable in moisture content conversions. The water vapor content varies with the amount of water vapor in the atmosphere and can change from 3.75 gm/m^3 to 15.0 gm/m^3 at sea level depending on the season and location. Normally standard values of 7.5 or 10 gm/m^3 are used.

5. Line Broadening Parameter

The line broadening parameter denotes the half power width (HPW) of the absorption line and is sometimes expressed in terms of wave number breadth denoted by $\Delta\gamma/c$, frequency width/velocity of light. For example, there are large number of narrow oxygen absorption lines in a band centered at 5 mm, a maxima about 2.5 mm and water vapor maxima near 1.35 cm, 1.63 mm and at very many (600) sub-mm wavelengths. Due to the line broadening effect these lines tend to merge into one diffuse band.

For vertical transmission through the atmosphere, the absorption coefficient in each spectral line varies from a very high value in the center of the line to a much smaller value on the sides. Also the effect on the absorption coefficient due to pressure, temperature and density (known as the broadening of absorption lines) is such that HPW of each line decreases steadily with increasing altitude. Most of the workers have considered only molecular collisions, whereas Meeks and Lilley [5] have included Zeeman effect above 40 km, and Doppler effect above 80 km, to calculate the broadening line widths.

For atmospheric absorption except at high altitudes, the decrease in pressure with height (1/2 atm. in the first 6000 m) is large enough to cause line width to be in the magnitude order of their separation and even of their center frequency. Under such conditions in actual atmosphere, the absorption calculated at any frequency which does not coincide

with a strong absorption maximum, is greatly effected by the wings of many overlapping lines and can widely vary depending on the broadening assumed for each of them. In spite of this complexity and evidence [6], most attempts to adapt the theory to the absorption measurements used only a single line broadening parameter throughout the absorption spectrum due to the lack of experimental verification and scarcity of information.

6. Variation of Water Vapor Content

The water vapor contained in the vertical atmosphere is described by the equivalent amount of precipitable cm water and this quantity varies depending on the latitude and altitude of a particular site. The data for 29 stations in the United States are taken from Weather Bureau tables [7] and presented graphically in figures 1 and 2 to show the general trend of dependence on latitude and altitude. The Weather Bureau report gives mean values of precipitable water. These mean values are averaged over layers of certain depths ranging between surface and 8 km altitude as well as over periods of one month.

In order to eliminate the altitude differences in the stations referred in the above report, the annual average of precipitable water from 3 to 8 km has been computed and presented as a function of latitude in figure 1. In the same figure the corresponding mean monthly values are plotted. The ratio between the maximum and minimum monthly mean values are about 3:1 (approximately independent of season). However, the ratio of maximum and minimum instantaneous values are considerably larger. Figure 1 reveals the general trend, that the amount of precipitable water decreases with increasing latitude.

Figure 2 shows the variation of annual mean precipitable water from surface to 8 km, with base altitude. The 29 stations are divided into five groups, each group member having approximately the same latitude. A straight line variation is drawn about the average value of each group, even though the individual values are changing at random. (For example, the increasing latitude of stations in two groups is shown by an arrow following a dotted line.)

From this figure one can see the precipitable water decreases with increasing altitude. It shall be noted that the Rocky Mountain area has the minimum amount of precipitable water.

Fig. 1 Variation of Precipitable Water with Latitude.

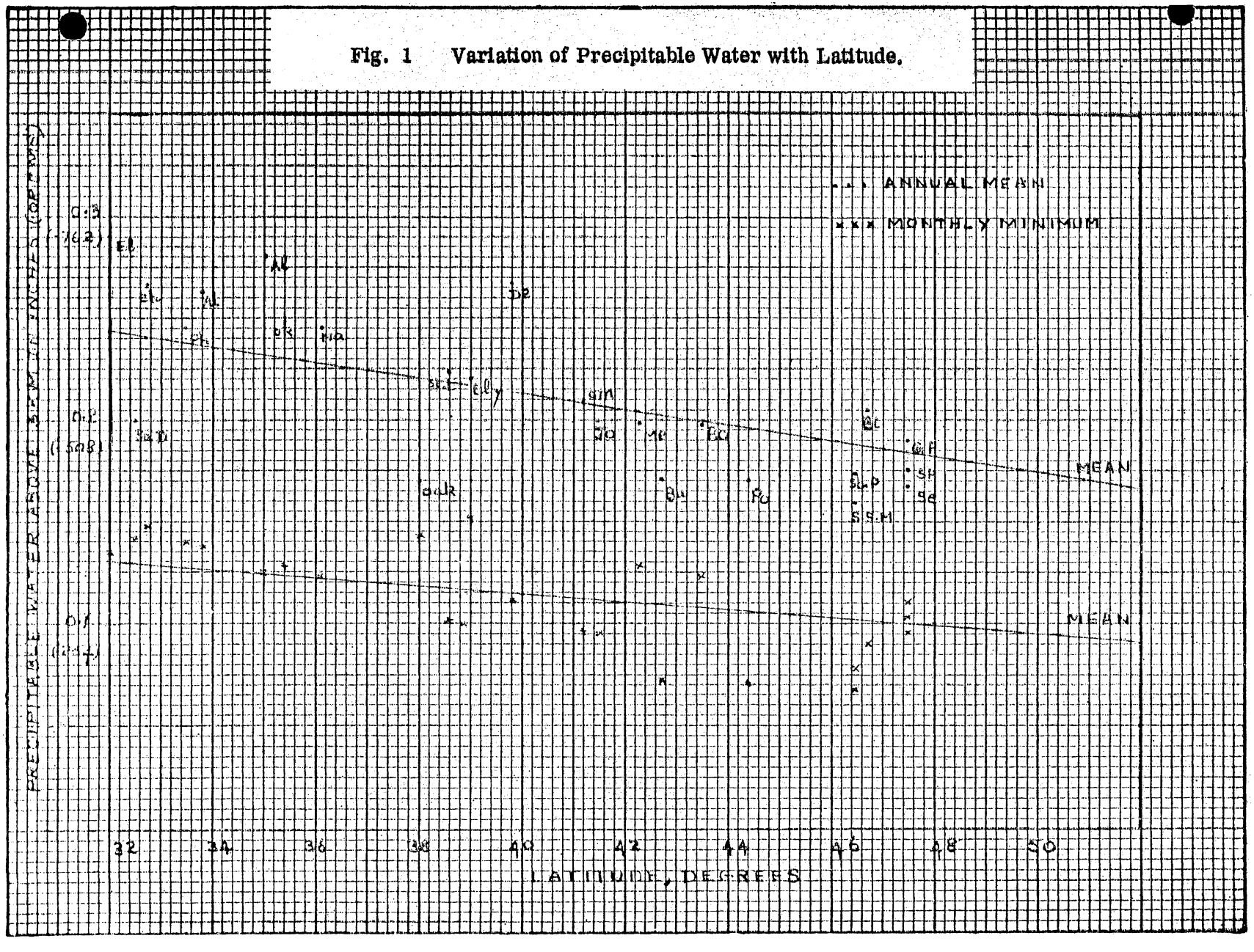

Fig. 2 Variation of Precipitable Water with Altitude.

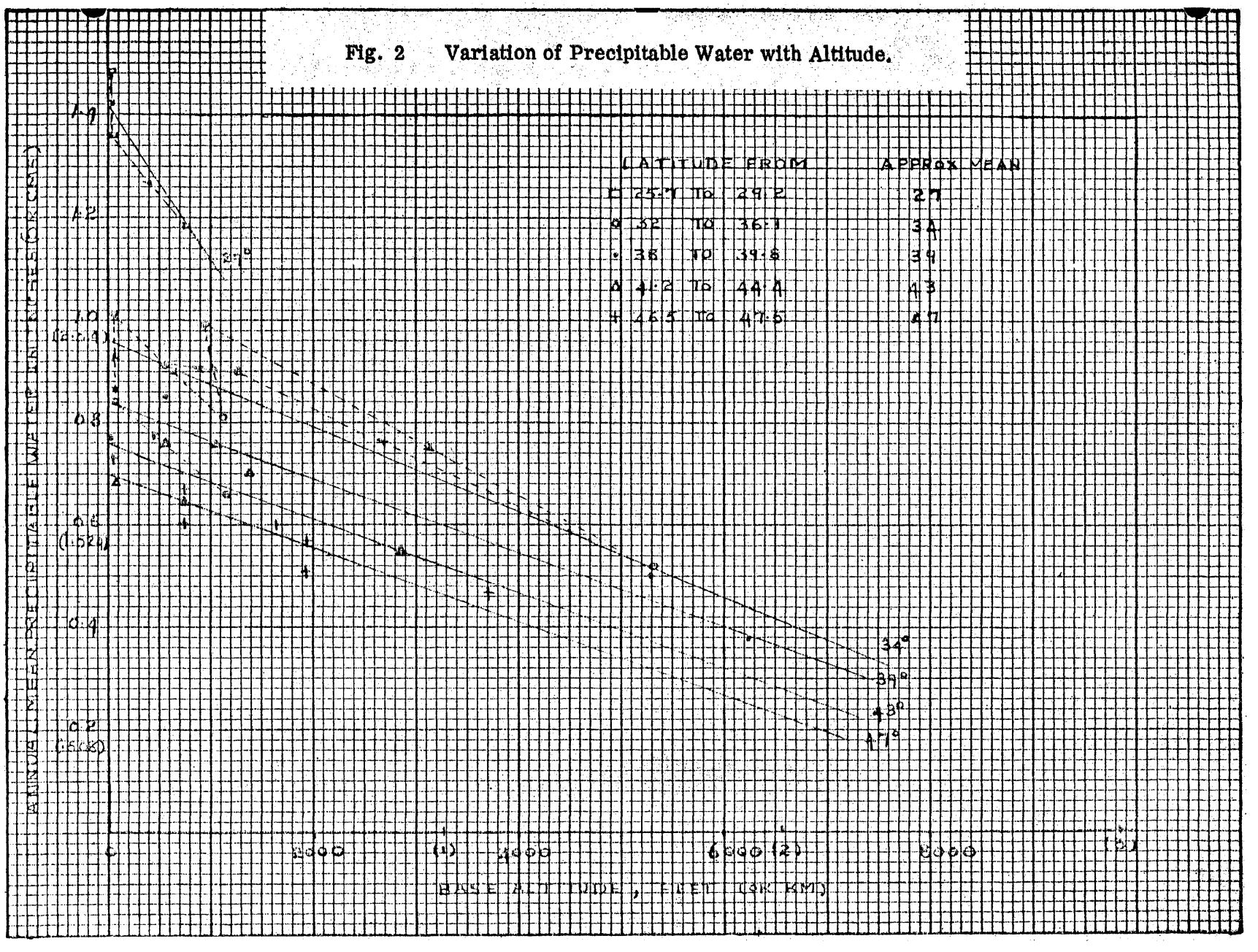

From these general observations, one can say that profitable experimental work from ground based antennas depends on the quality of the site chosen as much as the design of the instruments and one needs to choose a high mountain in a dry area (suitable geographic latitude) for an observatory site.

7. Methods of Absorption Measurements

The general experimental methods are described here. First, there are the convenient measurements over a chosen absorption path length between a laboratory transmitter and receiver. This has the benefit of ability to control the factors introduced in the absorption path, but in practice is hard to simulate actual atmospheric conditions. Also the path lengths should be quite large in order to obtain measurable attenuation specially in the wings of the absorption lines.

Second, quite a few absorption measurements at longer path lengths in km between ground based transmitter and receiver are available. The results give the horizontal attenuation (db/km) at a known atmospheric pressure but do not account for the vertical variations in the atmosphere. The atmospheric conditions over the entire propagation path are not uniform, as in the first case.

The third method determines the absorption through the entire atmosphere by measuring the radiation from bright extraterrestrial sources, like the sun, at different elevation angles. To compare these spectral results with theory, one has to assume the composition and other properties of the atmosphere as a function of altitude. Even though this procedure has the difficulty of separating the measured attenuation as due to different component contributions, based on theory, it has the benefit of giving the total vertical attenuation in a column of atmosphere (db) rather than attenuation per unit length (db/km). The results from these different measurements agree fairly well at frequencies of principal absorption maxima, for the major absorbants oxygen and water vapor.

8. Microwave Spectrum of Oxygen

Oxygen gas absorbs energy because the individual molecules behave like dipoles with a permanent magnetic moment. The incident electromagnetic wave passing over these molecules reacts with them, causing them to oscillate and rotate in a variety of ways. According to quantum theory, each of the vibrational states is associated with a certain energy level and is given by "$h\nu$". Thus it can be visualized that the incident wave delivers to the gas molecules discrete amounts of energy (in steps of "$nh\nu$") during the transition from the lower to the higher energy level. When the molecule returns to the lower level, it reradiates energy in all directions and only a small portion emerges in the propagation direction. The net result is an attenuation in the amplitude of the incident energy.

Figure 3 shows the horizontal oxygen attenuation for various elevations in the earth's atmosphere and is due to Rogers [8]. Thus it represents the gross changes in the absorption spectrum (50-70 kmcs) with increasing height. The various heights are representative of high pressure, transition and low pressure regions. It can also be seen that at the earth's surface the oxygen lines overlap completely to form a continuous region of absorption centered around 60 kmcs. At a height of 8-11 km, the lines continue to overlap, but some lines get clearer. At 30 km and above, the resonances due to individual rotation lines are resolved and the attenuation between the lines becomes quite small.

The oxygen absorption values in the horizontal direction at a given altitude, can be converted to other altitudes by using Van Vleck's [9] empirical relation,

$$L = L_O\left(1 - \frac{h + h_1}{20}\right) \tag{8}$$

where L and L_O are the horizontal path lengths and h is the height where the absorption has been measured, h_1 is the height to which this absorption value shall be converted. This formula for altitude correction holds good only in the lower atmosphere (up to 20 km). Using this relation one can see that the horizontal attenuation does not depend much on the altitude of any possible observation site. This is shown in the two lower curves of figure 4. The continuous curve shows the horizontal attenuation at Green Bank (0.83 km) based

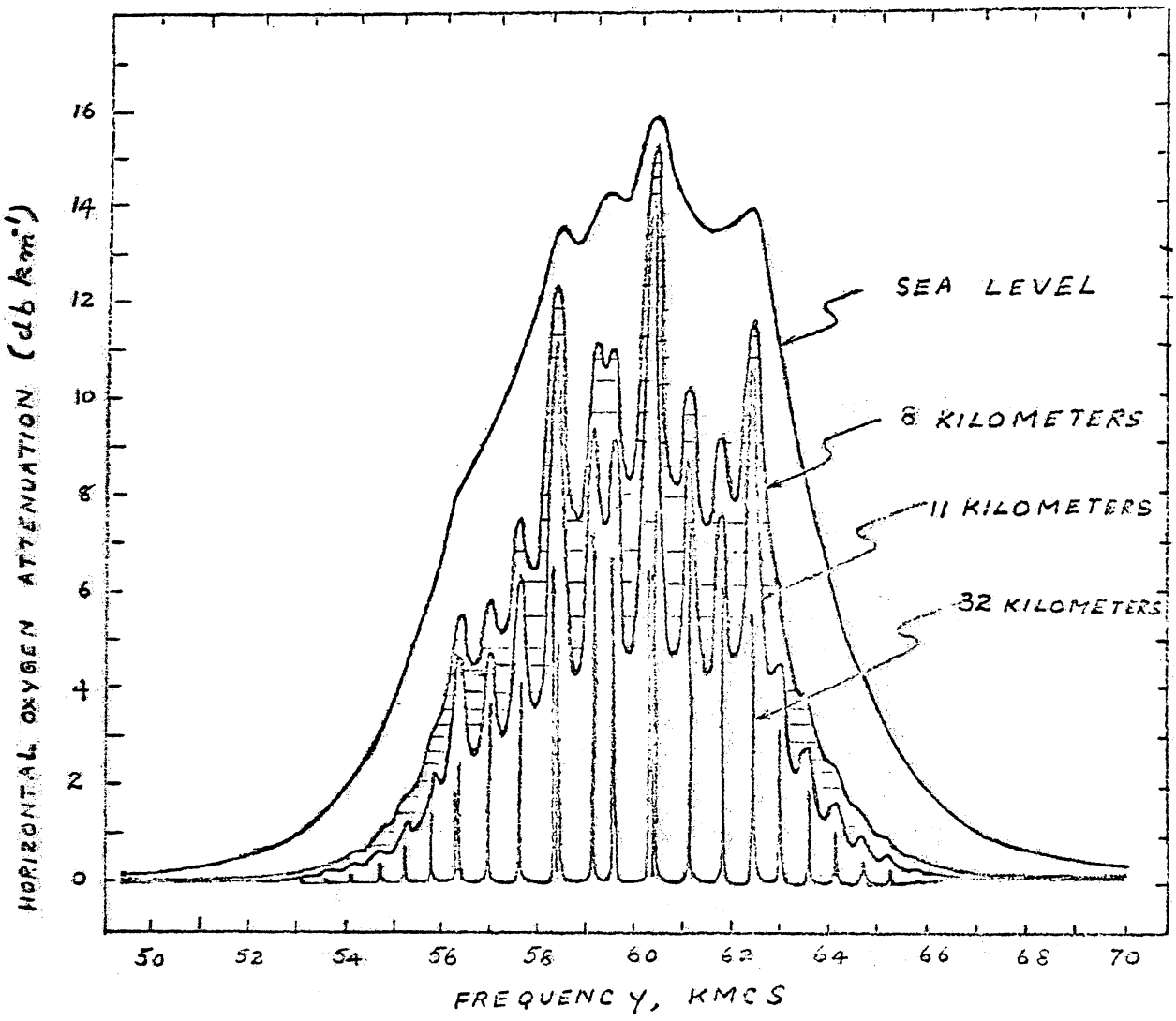

Fig. 3 Oxygen Attenuation for Various Elevations in the Earth's Atmosphere.

on Texas [10] sea level values. The dotted curve right below shows the horizontal attenuation at Climax (3.45 km) which is hardly different from the above.

Van Vleck [11] has theoretically estimated a single line broadening parameter, that can best approximate the observed line shape. Hogg [3] and Blake [12] used Van Vleck's theory with their own model atmospheres and measurements and their calculated attenuations are in fair agreement. Meeks and Lilley [5] are the only workers who based their theoretical calculations on a variable (0.01 to 100 mcs) line breadth parameter as a function of height (0 to 100 kms) in conjunction with ARDC model. They also considered the Zeeman (> 40 km) and Doppler (> 80 km) effects on the HPW. Rogers [8] also considered these effects.

The top curve in figure 4 shows the variation of calculated zenith attenuation with frequency (1-400 kmcs) due to Meeks and Lilley. Some measured values for cloudless conditions are shown and the range of values for some frequencies represent the spread in clear weather measurements. These are, however, mainly from astronomical observations and are due to the combined attenuation of water vapor and oxygen (there being no way to separate them). Thus the comparison with the selected experimental values with the theoretical curve shows that oxygen attenuation is predominant at these frequencies.

There is no simple relation between the measured attenuation in a horizontal path and the total absorption of the atmosphere in the entire frequency range. The empirical relation sometimes used, that the zenith attenuation of the atmosphere corresponds to the attenuation of a horizontal path of 5 km sea level length, seems to hold approximately at a few selected frequencies (like 35 and 140 kmcs). Tolbert, et al [13] also provide the calculated oxygen attenuation in the frequency range 20 to 300 kmcs based on $\Delta\nu = 1.9$ mcs per mm of Hg from absorption cell measurements. Their experimental spread of values at a couple of frequencies are in good agreement with the calculated attenuation and are denoted by T in figure 4.

Signal propagation in the vicinity of the line frequencies requires a detailed knowledge of the shape intensity and pressure broadening associated with that line. Also the measured attenuation can give information about the vertical thermal structure of the atmosphere.

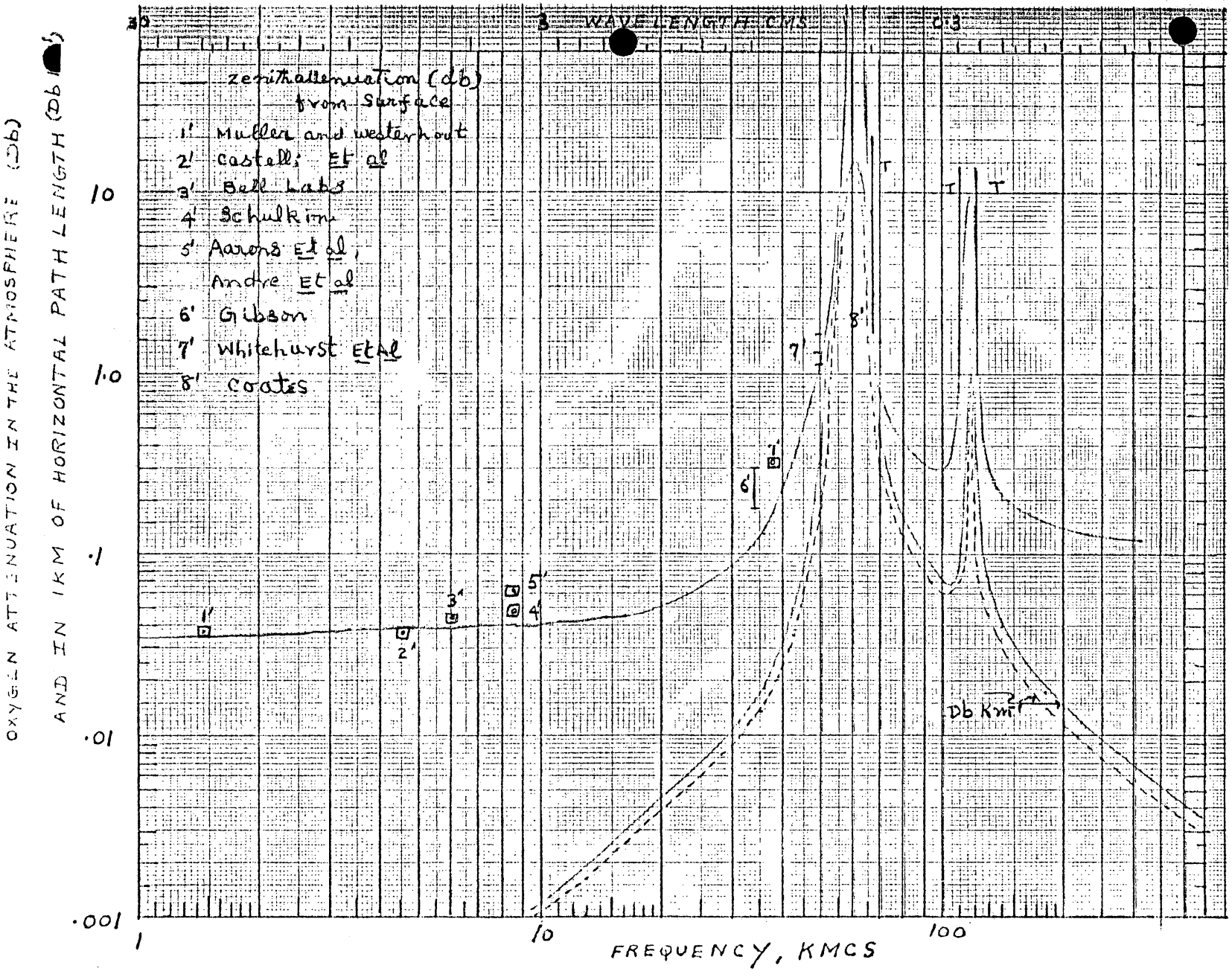

Fig. 4 Attenuation Due to Oxygen.

9. Water Vapor Attenuation

As pointed out before, even though water vapor comprises less than 3% of all gases, it absorbs nearly six times as much solar radiant energy as do all the other gases combined. Water vapor absorbs energy because the individual molecules behave like dipoles, and in the cm-mm region they have permanent electric dipole moment. These moments interact with incident electromagnetic energy to cause the molecular transitions that are responsible for the absorption.

The zenith attenuation calculations at any altitude are made on the basis of Texas group [10] values with the aid of Altshuler's plots of mixing ratio, relative humidity and precipitable cm, of water vapor variation with altitude. The water vapor mixing ratio is defined as the ratio of gms precipitable water vapor to kgms of dry air. The relative humidity is the ratio of observed mixing ratio to that which would prevail at saturation, at the same temperature. Since the pressure, temperature and density variations with altitude alter the water vapor absorption, the amount of water vapor in the line of sight can be equated to another value at sea level conditions (288 °K temperature and 760 mm pr.). Thus w_v represents the equivalent precipitable cms of water vapor in a vertical path from altitude h to ∞ and w_h represents the equivalent precipitable cms of water vapor in one km actual horizontal path length at an altitude h. Both w_v and w_h are corrected to sea level conditions and only w_v is useful in zenith attenuation calculations.

Figure 5 shows the horizontal water vapor attenuation [10] at sea level, 2, 4, 6, and 8 km elevations and horizontal oxygen attenuation at sea level in the frequency range 10 to 400 kmc. Using this horizontal attenuation (db/km) data for water vapor and oxygen, the attenuation through the entire earth's atmosphere can be determined theoretically by interpolating and extrapolating the attenuation values, to all elevations by use of modified Van Vleck-Weisskopf [14] (VVW) equation and commonly accepted ARDC atmospheric model. The horizontal attenuation values of water vapor in figure 5 are normalized to unit density. Hence, to obtain the total horizontal attenuation at each elevation, one has to know the corresponding density.

According to Altshuler, if the altitude of the tropopause changes, it will be assumed that the relative humidity will remain constant at 100% below the tropopause and the mxing ratio will remain constant above the tropopause. At sea level the water

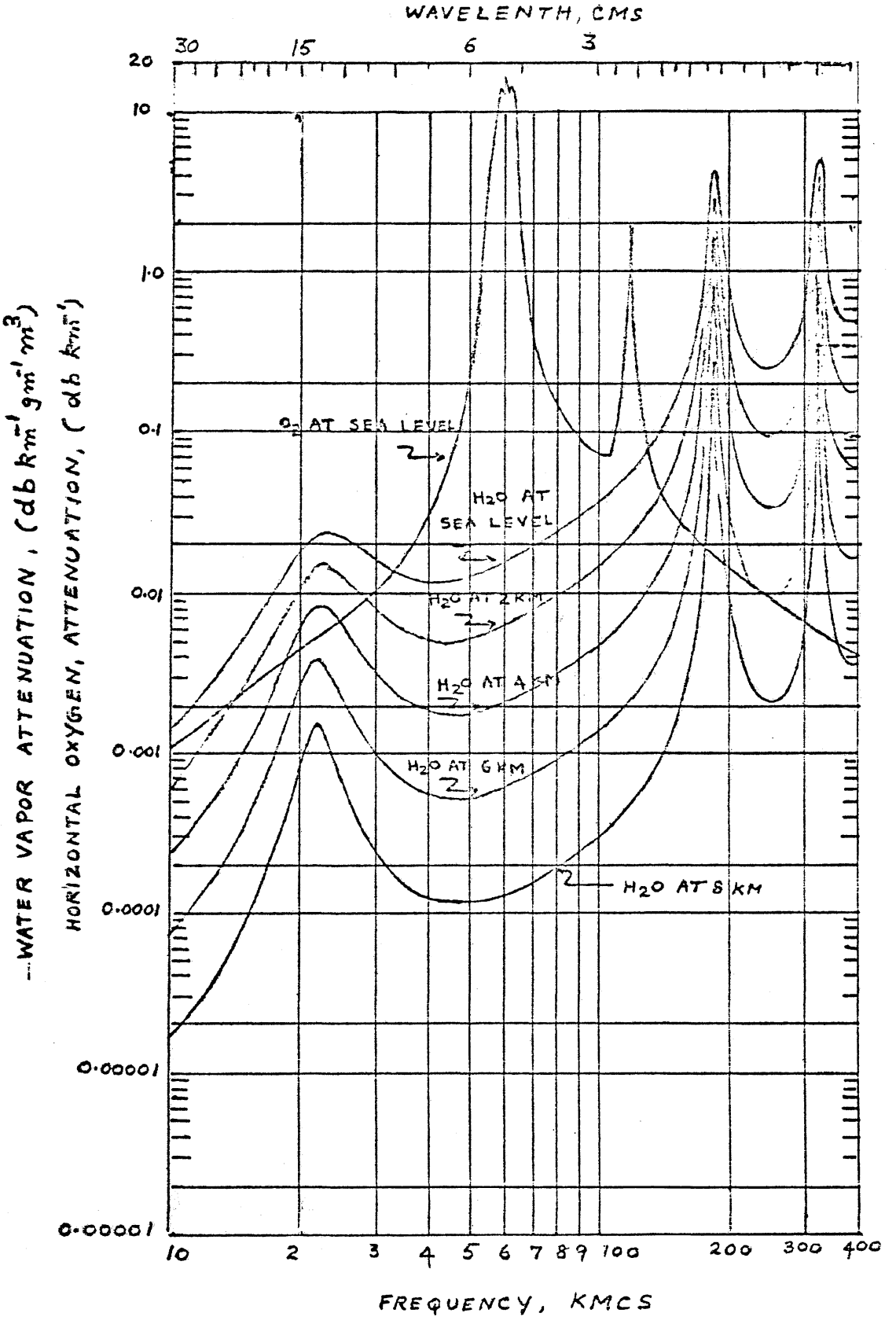

Fig. 5 Oxygen and Water Vapor Attenuation for Various Elevations in the Earth's Atmosphere.

vapor mixing ratio is 10 decreasing to 4.5×10^{-2} at 11 km, and remaining constant thereafter. From this knowledge of variation of water vapor mixing ratio and ARDC density variation of dry air, one can readily obtain the water vapor density variation with altitude. For an approximate estimate, the atmosphere can be considered to be made up of plane parallel layers of equal thickeness and with the knowledge of water vapor density at each layer. The total zenith attenuation from any altitude can be calculated.

After these calculations were completed a later article by Straiton and Tolbert [15] showed that their attenuation calculations were normalized to water vapor density of one gm m^{-3} at the surface. The total water vapor attenuation through the lower 9 km of the earth's atmosphere for different elevation angles from the earth's surface were given in the same frequency range 10 to 400 kmcs. They have assumed a rate of decrease of water vapor density with height in accordance with $e^{-0.5\,z}$, where z is the elevation in km. Thus the losses shown must be multiplied by the ground level water vapor density to obtain the total water vapor loss. With this given variation of water vapor density and altitude, one can obtain the zenith attenuation plots at any altitude. The values obtained from both Altshuler's model and the above empirical relation have been checked and found to agree quite well.

Figure 6 shows the variation of calculated zenith attenuation with frequency for different values of vertical precipitable cm, w_v, of water vapor. The Weather Bureau tables [7] based on monthly mean values, list maximum $w_v = 1.1$ cms and minimum $w_v = .24$ cms at Climax, Colorado. From Altshuler's plot these water vapor values correspond to altitudes of 1 km (1.2 cms) and 3.5 km (.24 cms), respectively. Sea level corresponds to $w_v = 2.1$ cms. Assuming a plane parallel layer atmosphere and using figure 5 with Altshuler's water vapor densities, the zenith attenuation in figure 6 is plotted for 10 to 400 kmcs for $w_v = 2.1$, 1.2 and .24 cms. From Altshuler's transmission data (with w_v as index), the zenith attenuation for a frequency range 150 to 10,000 kmcs is also plotted for $w_v = 1.0$ and .25 cms. One can compare the shifts in the frequency and the magnitude variation of attenuation over the two overlapping window regions, to get an idea of the differences from the two models used. Also from this comparison one can arrive at an approximate factor to match the curves at any w_v value.

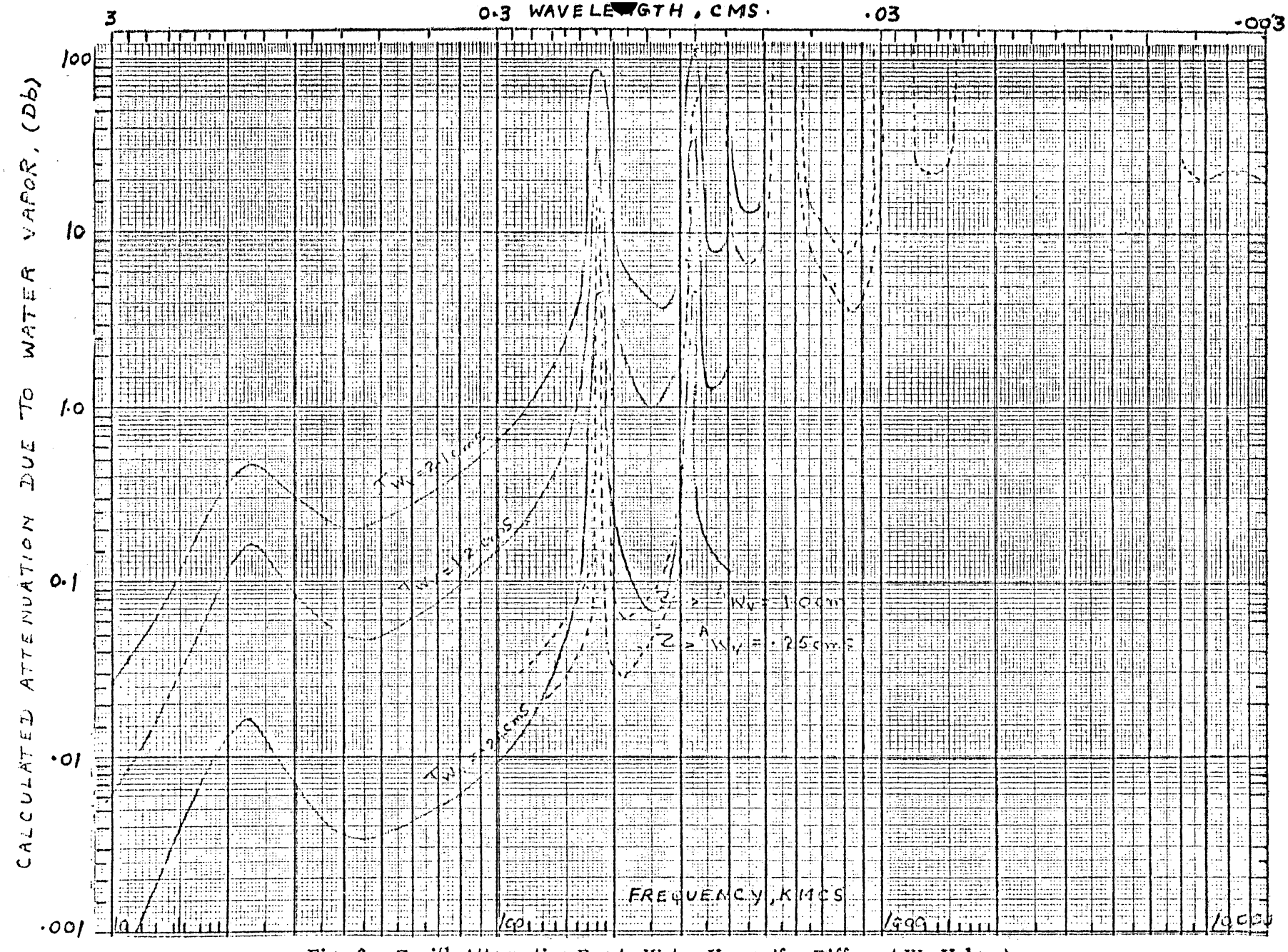

Fig. 6 Zenith Attenuation Due to Water Vapor (for Different W_v Values).

10. Total Zenith Attenuation

Figure 7 shows the zenith attenuation due to water vapor, oxygen and their sum at Green Bank. A rough measurement at Green Bank showed a variation of w_v from .35 to 2.0 cms over a few days. From Altshuler's model, 2.1 cms corresponds to sea level and 0.35 cms corresponds to 3 km. Again from the plane parallel atmospheric approximation for water vapor is plotted for w_v = 2.1 and 0.35 cms (surface up to 8 km) from 10 to 400 kmcs. Also, the zenith oxygen attenuation due to Meeks and Lilley [5] from sea level is plotted on the same figure from 1 to 400 kmcs. It is assumed that zenith oxygen attenuation observed at an altitude of 3 km is not different from zenith attenuation at sea level since measurements or calculations from various elevations in the entire frequency range considered are not available. The total attenuation plots are extended up to 1 kmcs by matching Blake's [12] values at 10 kmcs. This was possible for higher w_v = 2.1 cms. For lower w_v, this matching is not accurate, since attenuation due to oxygen very much exceeds water vapor attenuation in 1 to 10 kmcs region.

Two sets of zenith water vapor attenuation are plotted and the same sea level zenith oxygen attenuation is added to them separately to obtain two sets (for w_v = 2.1 and .34 cms) of total zenith attenuation. The center frequency, bandwidth, and attenuation values in the window regions are tabulated for the two cases.

For w_v = 2.1 cms

TABLE 2a

Center Frequency (kmcs)	Minimum Attenuation (db)	Bandwidth (kmcs)	Attenuation at Band Limits (db)
34	.35	30 - 38	(.4)
85	.8	70 - 100	(1.0)
135	1.8	125 - 145	(2)
260	4.	230 - 290	(5)
375	7.9	350 - 400	(8.4)

For w_v = 0.34 cms

TABLE 2b

95	.3	85 - 105	(.38)
147.5	.24	135 - 160	(.28)
250	.2	220 - 285	(.25)

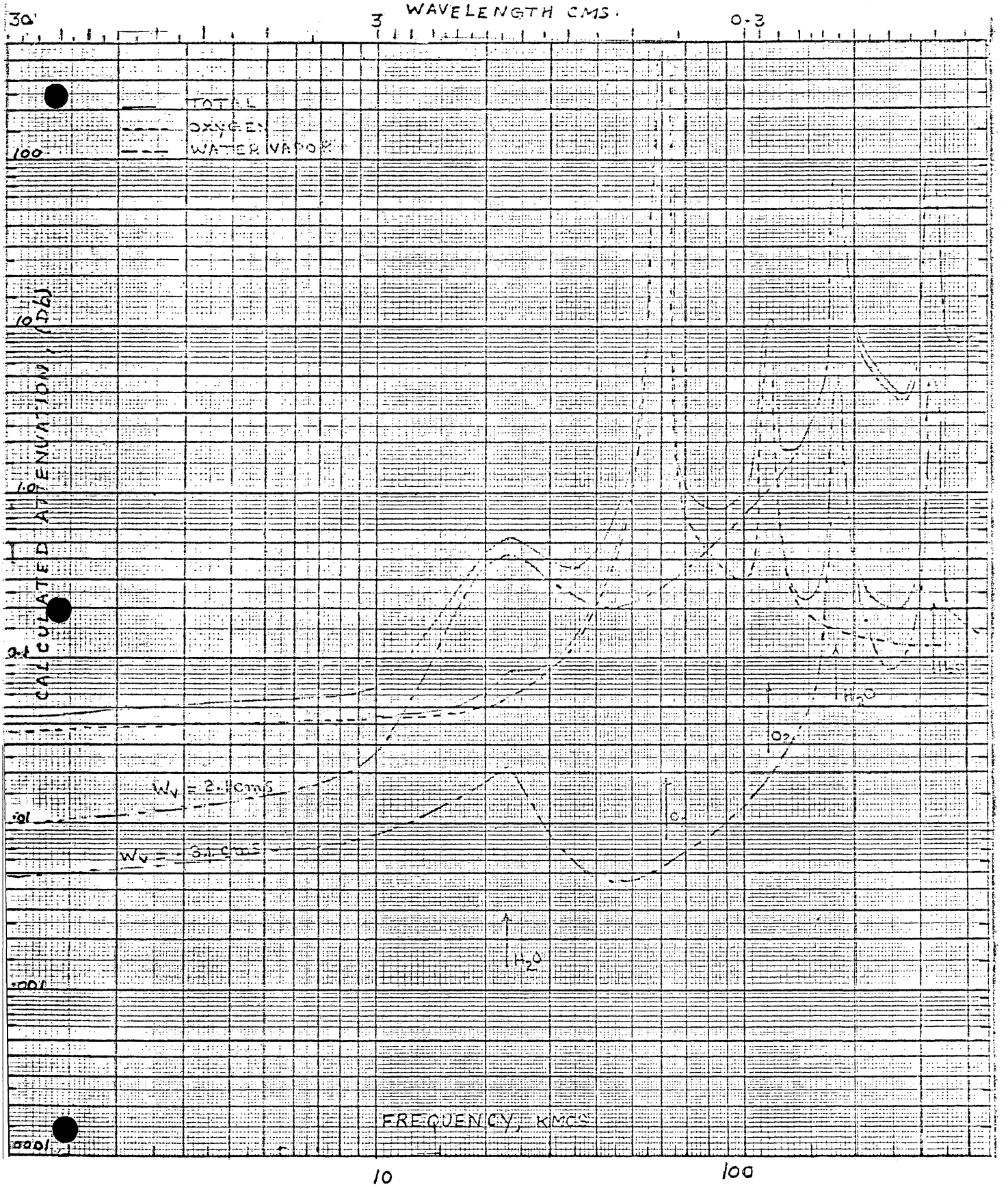

Fig. 7 Calculated Zenith Attenuation Due to Oxygen, Water Vapor and Their Sum.

Figure 8 summarizes the presently available calculated and measured total zenith attenuation values and the text explains some of their limitations. The continuous curve is the same calculated one shown in figure 7 (from sea level up to 8 km). Hogg presents the calculated values of total zenith attenuation through the atmosphere (0 to 20 km) from 14 to 40 kmcs. Hogg's curve shown dotted, used a different atmospheric model (described in section 2) and the VVW equation with parameters adjusted to fit the curve for transmission to zenith. Theissing and Caplan [16] give the attenuation values for zenith angle of 45° under the different water vapor conditions (dry, medium, and humid). This data is converted to zenith attenuation using the secant relation (equation (1)) and shown dotted in the figure. They used actual temperature, pressure and water vapor measured values. The source for the experiment was the sun and the detector was sensitive to an extended spectral range covering the sun's spectrum. The calculations were based on the integration of VVW equation over this spectrum, along with the observed parameters. The other available experimental data are also shown in figure 8 with the letters indicating the names of the authors after Rosenblum [17]. It can be seen that the general agreement in the location of windows and the order of attenuation magnitudes (other than at resonances) are comparable.

11. Zenith Attenuation from 1 to 20 Microns

It has been found from quantum mechanical analysis that the far infrared and millimeter wave absorptions are associated with purely rotational states of molecules. The molecular bands in the infrared over the spectral region 1-20 microns arise from vibrational states of the atoms within a gas molecule. A molecule in a given energy state can absorb those wavelengths of radiation which correspond to the allowed quantum transitions to some other energy states. The absorption corresponding to one set of initial and final rotational energy states gives rise to a spectral line, and the entire ensemble of rotational lines associated with the transitions between two vibrational energy states is called a vibration-rotation band. The width of the spectral lines depend on the temperature and pressure in a complex way.

The infrared absorbers are water vapor, CO_2, O_3, N_2O, CH_4, and CO. Near the ground the principal absorbers are H_2O and CO_2. Ozone is not distributed uniformly

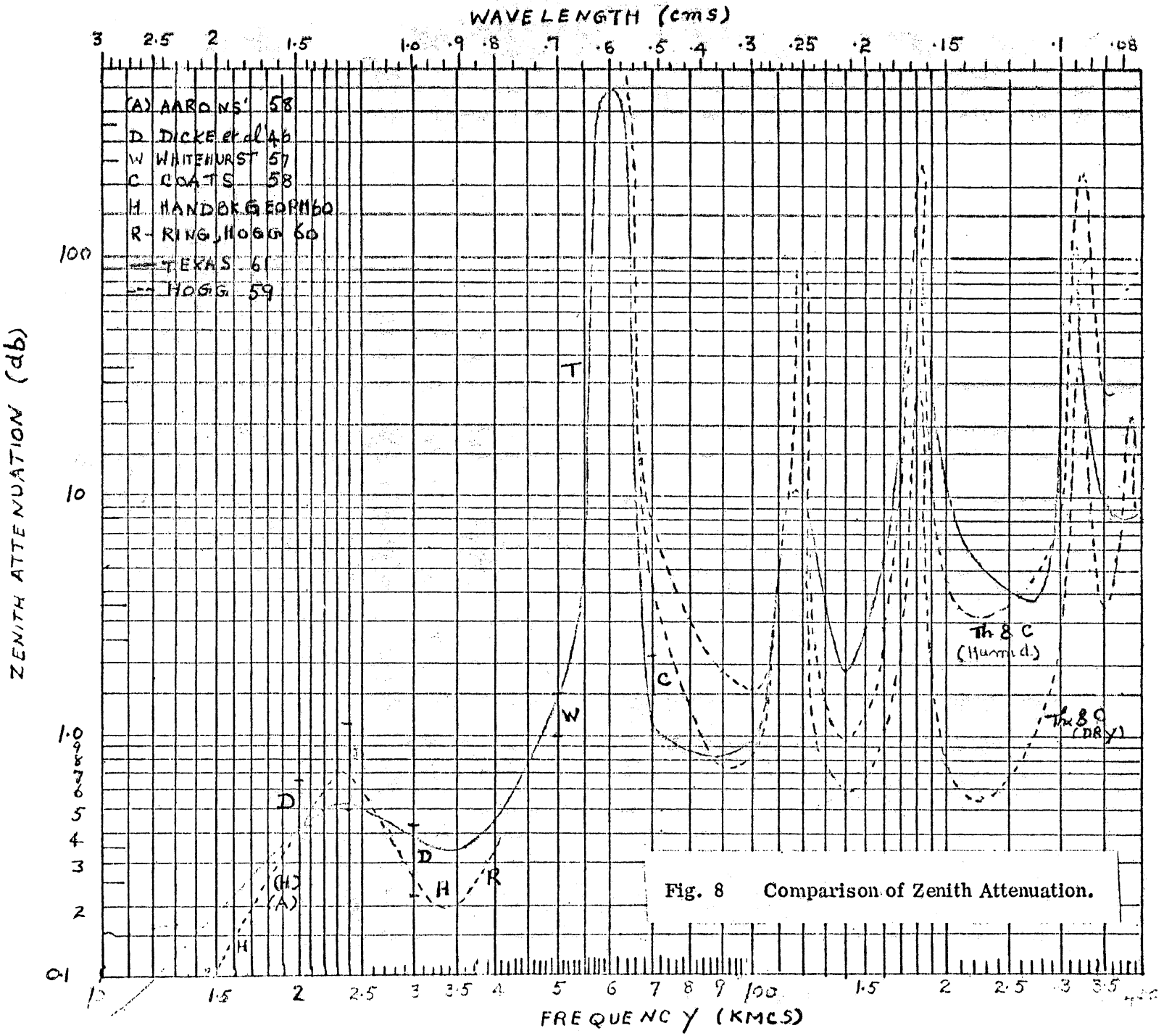

Fig. 8 Comparison of Zenith Attenuation.

through the atmosphere, but is mostly concentrated between 10 and 40 km above the earth's surface, with significant peak at about 20-30 km. Ozone shows a large variation with latitude season and weather conditions. The minor constituents CH_4, N_2O and CO, like CO_2 are found to be uniformly distributed throughout the atmosphere (as shown in Table 1, section 3). Water vapor is the most variable in its concentration in the atmosphere, because the humidity of air fluctuates widely with geography, seasons and the time of day, most of it being near to the ground level.

As a major aid in the calculation of infrared transmission Altshuler [1] has published a detailed procedure for the determination of the infrared line of sight (geometry with respect to earth) and for the evaluation of amount of gases, vapors and haze in the line of sight. Gases and water vapor absorb infrared radiation in regions of their vibration-rotation bands. Temperature and pressure will effect the width of the spectral lines which will then alter the degree of absorption of infrared by the gas. Hence, relative to its infrared absorption, the amount of gas in the line of sight can be equated to another amount under sea level conditions (288 °K temperature and 760 mm · Hg pressure). This sea level amount is termed the "equivalent amount of gas in the line of sight, corrected to sea level conditions".

Thus d denotes the equivalent path length of dry air in the infrared path, corrected to sea level conditions, in km. This is used as an index to specify amounts of CO_2, N_2O, CH_4, CO and haze, which have approximately constant mixing ratios with air, from 0 to 50 km altitude. w represents the equivalent precipitable cm of water vapor and z equivalent atmospheric cms of ozone, in the line of sight corrected to sea level conditions. Small lettered subscripts v and h refer to vertical and horizontal paths as used to describe w_v and w_h. In the present case, as we are mainly interested in the zenith attenuation alone, the line of sight is essentially vertical and d_v, w_v and z_v become d, w and z, respectively. Altshuler gives these equivalent sea level path lengths versus altitude to be used as an index to determine appropriate transmission from the transmission-frequency data.

Figure 9 makes use of the suggested Altshuler's procedure, as outlined above, to obtain zenith attenuation at Climax (3.44 km), Colorado. The attenuation due to water vapor, CO_2, N_2O, O_3 and scattering are considered as the transmission data for these

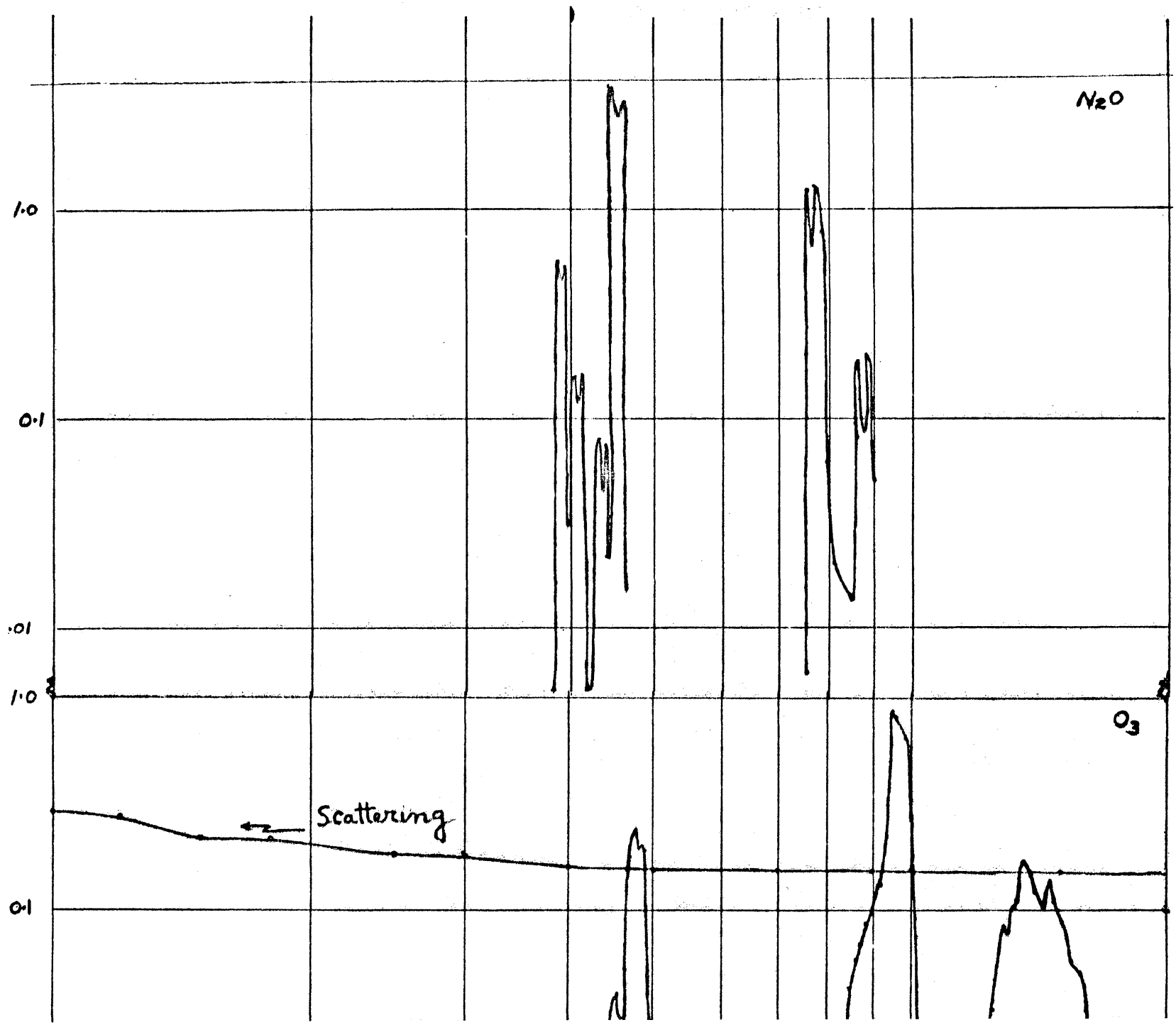
1.0
0.1
.01
1.0
0.1
N2O
O3
Scattering

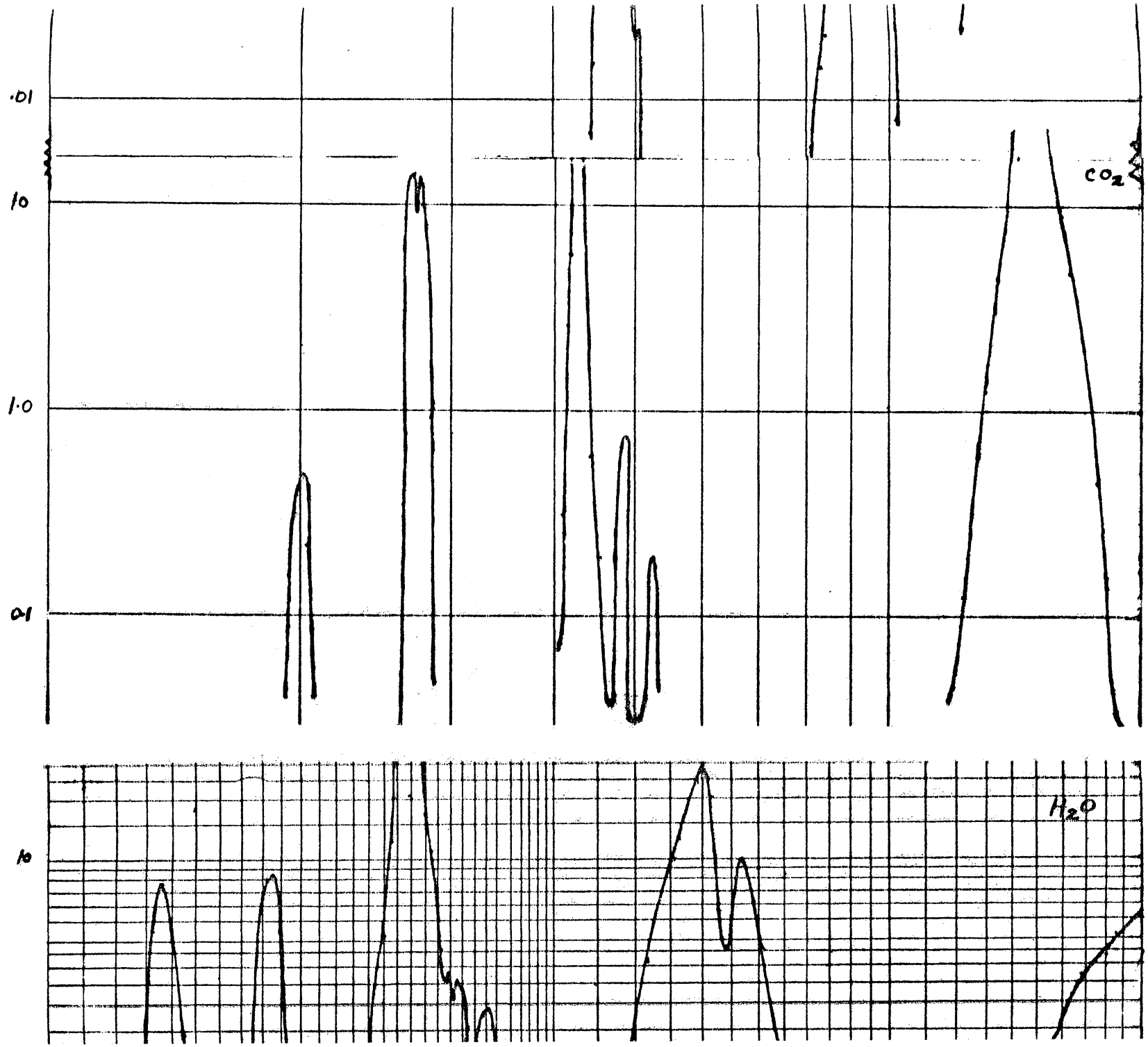
.01
10
1.0
.1
CO_2
10
H_2O

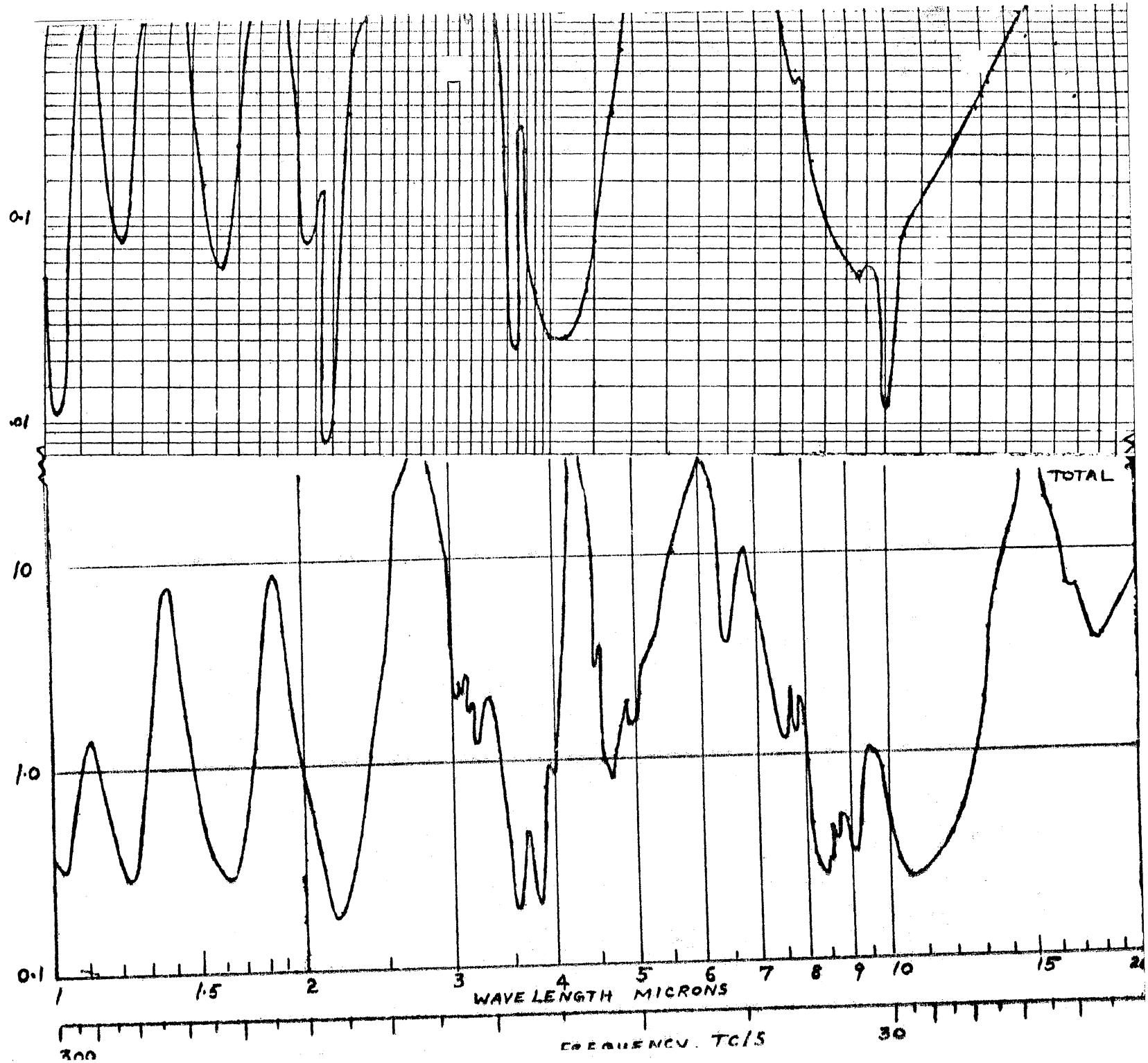
0·1
·01
10
1·0
0·1
TOTAL
1
1·5
2
3
4
5
6
7
8
9
10
15
WAVE LENGTH MICRONS
300
30

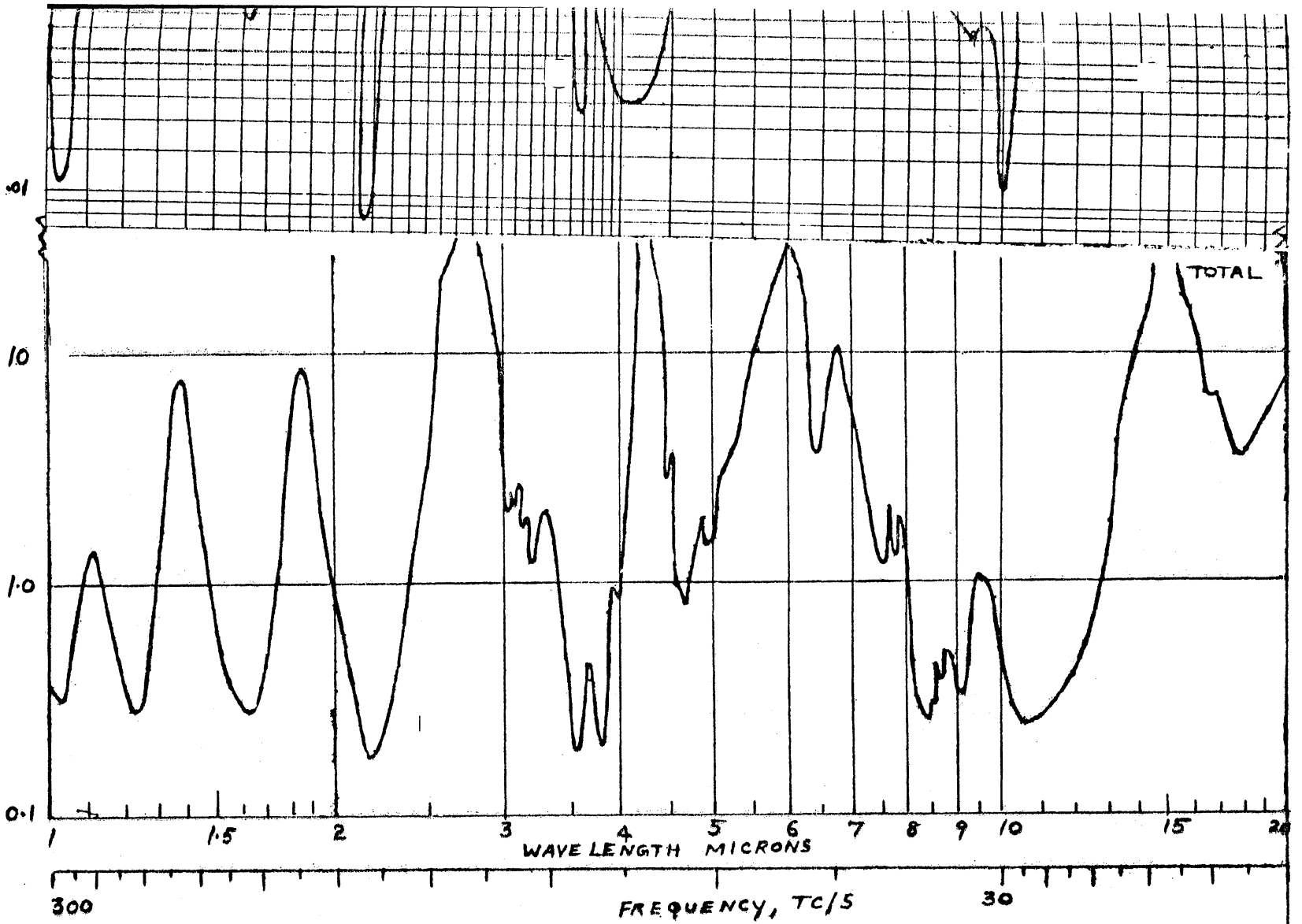

Fig. 9 Zenith Attenuation From 1 to 20 Microns Due to H_2O, CO_2, O_3, N_2O, Scattering and Their Sum.

constituents only are available. The absorption bands for CH_4 and CO are so weak in comparison with other absorbers that they are not considered to affect the atmospheric transmission sufficiently. Figure 9 thus shows the zenith attenuation for H_2O, CO_2, N_2O and O_3 over a wavelength 0 to 20 microns. It can be seen that so far as water vapor is concerned the major windows are in the 8-14 μ, 3.7 to 4.5 μ regions and some narrow ones below 3 microns. There is limited transparency from 14 to 25 μ, and from 25 to approximately 1000 μ, the earth's atmosphere is made almost opaque by the pure rotational spectrum of water vapor. CO_2 is the next major absorber with absorption bands around 15 μ, 4.3 μ and 2.8 μ, contributing fairly large amounts of attenuation. O_3 and N_2O also have few absorption bands but they contribute a minor loss of order of a db at the peaks. Also CH_4 and CO do have strong absorption bands in the lower 1-6 μ spectral region as evidenced from the infrared solar spectrum. But here it is assumed they do not contribute much to the total attenuation. Scattering varies a little from 1 to 4μ and later remains constant about 0.1 db up to 20 μ. From extinction measurements the common radii for haze are between 0.3 to 0.4 μ and the empirical Rayleigh scattering varies as lower power of λ (order 0 to 1) and hence contributes very little to the attenuation.

According to Altshuler's report the water vapor absorption blocks more or less completely any observation in the wavelength region between 180 to 50 micron (as shown in figure 6). Because of the lack of sensitive detectors for this wavelength region, very few experimental results [18, 19] are available. Figures 10 and 11 show some of this experimental data obtained by Yaroslavsky and Stanevich [18], Gebbie [19] and from these, one may be able to find some more useful observation windows in the sub-mm and far infrared region. Figure 10 gives the optical density (relative transmission) of atmospheric air, in the laboratory, for a layer of thickness 10 meters at a temperature of 20 °C, pressure of 760 mm Hg and absolute humidity 10.5 gm/m^3. In Figure 11, the observations were made with a two-beam interferometer of 30 cm aperture and a Golay-type thermal detector. Spectra were obtained from the interferograms by digital computation.

There are some complete review articles [20, 21] on the transmission of the atmosphere in the infrared and a few high resolution spectral [22] measurements. The spectral data usually show the positions and relative intensities of the molecular absorption bands in the atmosphere, whereas figure 9 gives the absolute attenuation values due

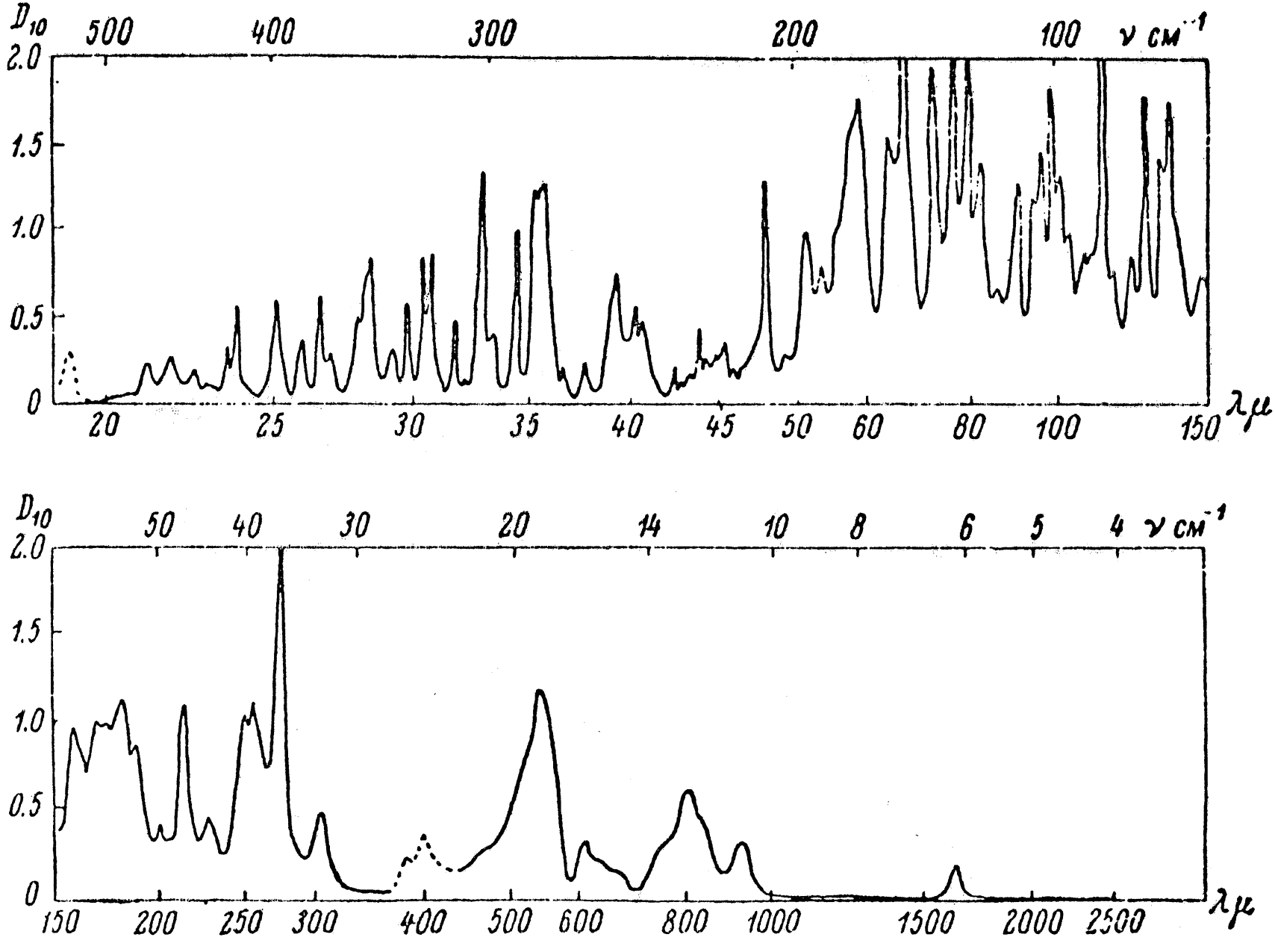

Fig. 10 Measured Relative Transmission in the Far Infrared Region (20-2500 μ) for a Layer of 10 Meters Thickness [18].

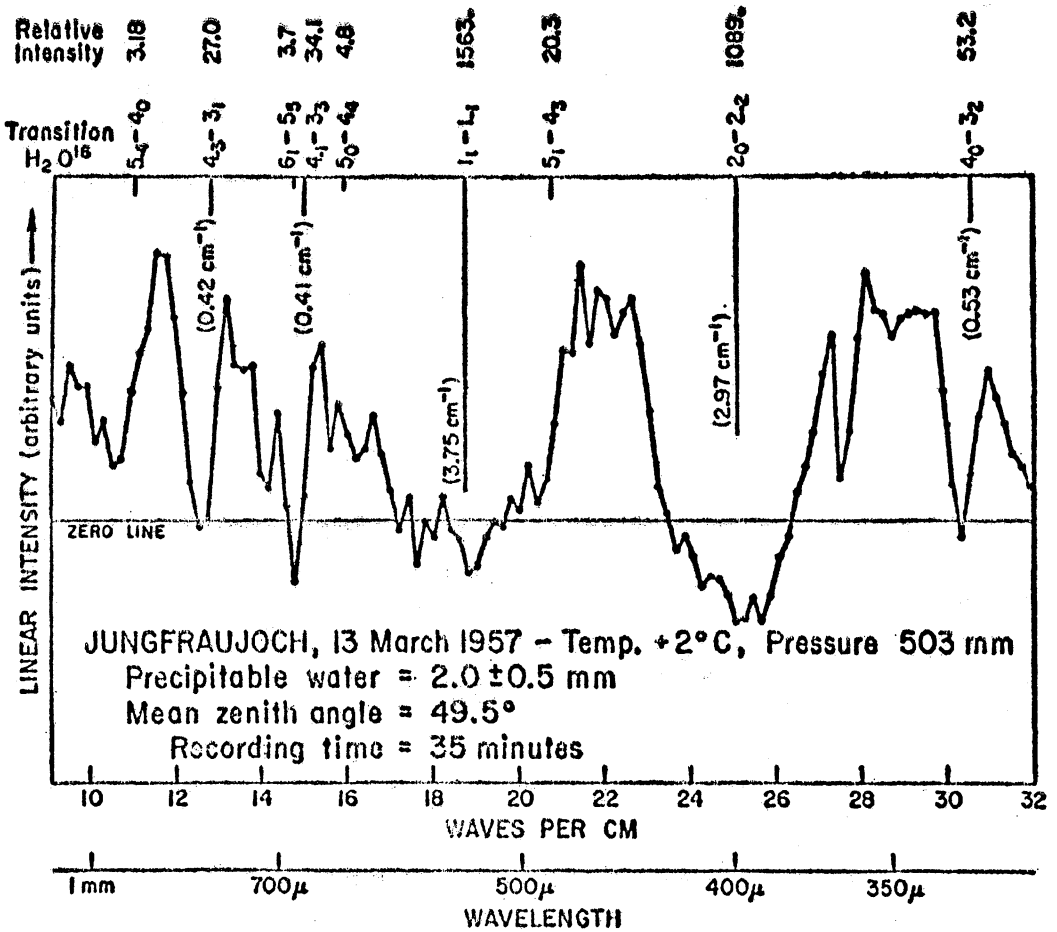

FIG. 11. Submillimeter spectrum of solar radiation showing regions of atmospheric transmission and absorption. The calculated positions and intensities of pure rotation lines of H_2O are given. The numbers in parentheses are calculated half-widths for selected lines. [19]

to various components and their sum, which provides a better means to compare the losses in the various frequency regions.

Acknowledgement

The author wishes to express her appreciation of the many valuable discussions with Dr. Peter Mezger.

12. Appendix: Van Vleck-Weisskopf Theory

The theory of pressure broadening was first proposed by Lorenz [23]. Lorenz treated resonant absorption, while Debye [24] treated nonresonant absorption. It was anticipated that Debye's theory would turn out to be a special case of Lorenz theory. However, this supposition was not true and the need for further clarification arose. A single integrated absorption theory was put forward by Van Vleck and Weisskopf [14] by combining both the above theories with modified assumptions. For a single absorption line due to any gaseous constituent, the attenuation α, at an angular frequency ω associated with pressure broadening is given by VVW equation

$$\alpha = \frac{2\pi Ne^2}{mc} \left|\frac{\omega}{\omega_c}\right|^2 \left[\frac{1/\tau}{(\omega - \omega_o)^2 + (1/\tau)^2} + \frac{1/\tau}{(\omega + \omega_o) + (1/\tau)^2}\right]. \tag{9}$$

Here e and m are the charge and mass of an electron, c is the velocity of electromagnetic wave, ω_o is the angular frequency of the center line, N is the number of molecules per cubic cm and τ is the mean interval between collisions. The term $(1/\tau)$ may be replaced by $\Delta\omega$, the half width of the line at its half power point.

The contributions to the absorption from the various lines may be obtained by adding their individual attenuations. The number of molecules per cubic cm and the line width can be seen approximately proportional to pressure. The line breadth parameter $\Delta\nu = \frac{\Delta\omega}{2\pi}$ was left as an undetermined factor in this equation. This is best found by actual atmospheric measurements. The more recent work on collision broadening has been directed toward deriving more explicit expressions for $\Delta\nu$. The intensity distribution in a pressure broadened line is represented by Fourier expression, to obtain a formula for the line breadth and the line shift of a spectral line [25]. Van Vleck subsequently modified the VVW equation for the microwave absorption of oxygen and water vapor by adding another term to equation (9) to account for the residual effect of neighboring lines besides the main absorption maximum.

According to Van Vleck [11] the oxygen absorption in the range 0.7 to 10 cms is proportional to the square of the pressure and at shorter wavelengths the absorption is

independent of pressure. The attenuation increases gradually with the decrease in temperature. At -40 °C the attenuation is about 78 percent higher than at 20 °C. Schulze and Tolbert [26] have studied the details of the shape, intensity and pressure broadening of 2.53 mm oxygen absorption line wing in detail. There is discrepancy between these measurements and VVW theory, probably due to an inappropriate choice of line shape factor to describe the losses in the wings of absorption lines.

Van Vleck's quantum mechanical calculation for water vapor [27] in the 0.07 to 10 cms range shows that the combined residual attenuation due to neighboring lines around 1.35 cm is inversely proportional to pressure. The attenuation is directly proportional to pressure at other wavelengths. Attenuation increases slowly with decreasing temperature and is 20 to 45 percent greater at -40 °C that at 20 °C. The measured attenuation due to residual effect is found to be four times larger than predicted value. Tolbert, et al [13] made atmospheric measurements in the 100-140 kmcs range. They also found that the actual atmospheric values are four times larger than theoretically anticipated. This discrepancy can either be due to the assumption of Lorenz model of infinitely sharp collisions, or inappropriate line width factors.

VVW theory assumes the period of oscillation of incident energy to be much longer than the mean duration of a molecular collision. This is true for microwaves but becomes worse as the incident radiation frequency increases. Molecular collision broadening is considered for the prediction of effects of pressure and temperature on line broadening. Thus the VVW theory and the modifications have been able to account quite well for the observed maxima of oxygen and water vapor. However, the values of the actual atmospheric attenuation in the wings of the lines do not agree with theoretical values due to the complexities in the pressure broadening effects.

References

[1] Altshuler, T. L., "Infrared and Background Radiation by Clear Atmosphere", General Electric, Doc. No. 61SD199 (December 1961).

[2] "Handbook of Geophysics", Macmillan Co. (1960).

[3] Hogg, D. C., J. App. Physics, 30, p. 1417 (1959).

[4] Byers, H. R., "General Meteorology", McGraw Hill (1959).

[5] Meeks, M. L. and Lilley, A. E., "The Microwave Spectrum of Oxygen in the Earth's Atmosphere", Harvard College Observatory, HRAP-105.

[6] Benedict, W. S. and Kaplan, L. D., J. Chem. Phys., 30, p. 388 (1959).

[7] Shands, A. L., "Mean Precipitable Water in the United States", Weather Bureau, Technical Paper No. 10.

[8] Rogers, T. F., Phys. Rev., 93, p. 248; 95, p. 622A (1954).

[9] Van Vleck, J. H., "Propagation of Short Radio Waves", p. 647, Radiation Lab Series (1951).

[10] Tolbert, C. W. and Dickinson, R. M., "Calculated Values of Absorption Due to Water Vapor and Oxygen in the Millimeter Spectrum", Elec. Eng. Research Lab., University of Texas, Report 6-42 (February 1961).

[11] Van Vleck, J. H., Phys. Rev., 71, p. 413 (January-June 1947).

[12] Blake, L. V., "Tropospheric Absorption and Noise Temperature for a Standard Atmosphere", Naval Research Lab, PT-GAP International Symposium (July 1963).

[13] Tolbert, C. W., Krause, L. C., and Straiton, "Attenuation of the Earth's Atmosphere Between the Frequencies of 100 to 140 Gc/s", to be published in J. Geophysical Research in 1964.

[14] Van Vleck, J. H. and Weisskopf, V. F., Rev. Mod. Phys., 17, p. 227 (1945).

[15] Straiton, A. W. and Tolbert, C. W., IEEE Transactions, Vol. MTT-11, p. 296 (September 1963).

[16] Theissing, H. H. and Caplon, P. J., JAP, 27, p. 538 (1956).

[17] Rosenblum, E. S., Microwave J., Vol. 4, No. 3, p. 91 (March 1961).

[18] Yaroslavsky, N. G. and Stanevich, A. E., Optics and Spectrascopy, 7, p. 380 (July-December 1959).

[19] Gebbie, H. A., Phy. Rev., 107, p. 1194 (1957).

[20] Howard, J. N., Proc. IRE, 47, p. 1451 (1959).

[21] Howard, J. N. and Garing, J. S., Infrared Physics, 2, p. 155 (1962).

[22] Gates, D. M. and Harrop, W. J., App. Optics, p. 887 (September 1963).

[23] Lorentz, H. A., Proc. Amst. Sci., 8, p. 591, 1906.

[24] Debye, P., "Polar Molecules", Chapter 5, Dover Publications.

[25] "Opacity of the Atmosphere at Millimeter Wavelengths", University of Alabama, Research Institute, FTR-1 (January 1962).

[26] Schulze, A. E. and Tolbert, C. W., Nature, 200, p. 747 (1963).

[27] Van Vleck, J. H., Phys. Rev., 71, p. 425 (1947).

COLLECTED ARTICLES AND DATA RELEVANT to the DEVELOPMENT AND OPERATION of the NRAO INFRA-RED HYGROMETER commonly known as the LOW METER

M. A. Gordon
National Radio Astronomy Observatory
Tucson, Arizona

June 6, 1986

(10 copies)

Foreword:

The Low portable water meter has been an important instrument in regard to site surveys for radio and infra-red astronomy. I believe that the value of the instrument lies (1) in simplicity and ruggedness of its design and (2) in the choice of a water-vapor band having a dynamic range appropriate for evaluating astronomical sites. Its accuracy is also well-matched to the intrinsic sampling errors unavoidable in most site surveys of atmospheric water vapor.

Unfortunately, most of its development is chronicled in unpublished papers and internal reports which can be easily lost from astronomical history.

This report is a collection of the fundamental articles, reprinted from the rare and often dog-eared copies in my files. I hope that this anthology will preserve the history of the Low meter for a little longer.

-- M. A. Gordon

Table of Contents

Paper 1: "A Spectral Hygrometer for Measuring Total Precipitable Water", by N. B. Foster, D. T. Volz, and L. W. Foskett.

This is a fundamental reference for the measurement concept. It includes the empirical relationship between radiosonde observations of water vapor and the IR ratio used to calibrate the Low meters.

Paper 2: "A Comparison of Mean Precipitable Water-Vapor at Several Selected Locations Using An Improved Type Water-Vapor Hygrometer", by F. J. Low.

This include the first results of the portable Low meter, the original distribution list for the meters, and the calibration curve for model A(3-1). Gerard Kuiper carried A(3-1) to many sites world wide. It was used for the LBL reports on water vapor written by Kuiper. Its zero-point calibration was made by Francis Gary Powers from a U2 aircraft over Tucson, Arizona. This meter, now broken, was in the possession of Arnold Davidsen in Tucson as of January 1986.

Paper 3: "Measurements of Atmospheric Attenuation at 1 Millimeter and a Description of a Portable Spectral Hygrometer", by F. J. Low and A. W. Davidsen.

This paper gives a detailed technical description of the fixed and portable Low meters and reports some observational results of the fixed meter.

Paper 4: "Calibration of an Atmospheric Water Vapor Meter by Means of Synthetic Spectra", by T. N. Gautier and U. Fink. This important but unpublished work confirms that the square-root of pressure correction is appropriate for measurements taken with the 0.935 micron band. (It is not correct for other water bands, however).

Data: The spectral transmission of the filters for Low meter "C", resident at the NRAO 12-m telescope on Kitt Peak. The filters of this instrument have changed little since it was built.

This paper, printed in its present form as a manuscript in limited quantity, was presented at the 1963 International Symposium on Humidity and Moisture, Washington, D. C., May 20-23, 1963. As this reproduction does not constitute a formal scientific publication, any reference to the paper in published articles and scientific literature should identify it as a manuscript of the U. S. Weather Bureau.

UNITED STATES DEPARTMENT OF COMMERCE

WEATHER BUREAU

A SPECTRAL HYGROMETER FOR MEASURING TOTAL PRECIPITABLE WATER

by

Norman B. Foster and David T. Volz
Physical Science Laboratory

and

Laurence W. Foskett
Instrumental Engineering Division

Washington 25, D. C.

June 1963

A Spectral Hygrometer for Measuring Total Precipitable Water

by

Norman B. Foster, David T. Volz, and Laurence W. Foskett

U. S. Weather Bureau, Washington, D. C.

ABSTRACT

This paper describes a recording photoelectric spectral hygrometer developed by the U. S. Weather Bureau for determining the amount of water vapor in a vertical column of the atmosphere. Basically, the hygrometer monitors the relative radiant intensity of direct solar energy transmitted in a water-vapor absorption band. A sensing path directed at the sun is maintained by means of a motor-driven equatorial mounting.

The intensity of the radiation in the selected region of absorption is compared to that of a nearby

region having essentially no absorption. The region of absorption is centered at 0.935 micron and the reference region at 0.881 micron. Narrow-band-pass interference filters isolate the two spectral regions. Silicon solar cells are used as radiation detectors.

The instrument is designed so that the ratio of the photocurrents is proportional to the ratio of the transmitted radiant energies. Continuous ratio measurements are automatically obtained on a recording, self-balancing ratio bridge. Calibration depends on an empirical method involving simultaneous values of total precipitable water calculated from radiosonde observations.

Both laboratory tests and trial operation have demonstrated the dependability of the spectral hygrometer. Its stable design makes it suitable for use in the operational activities of meteorology as well as in research.

1. Introduction

Those interested in forecasting precipitation have for many years felt the need for a field instrument that would provide a continuous record from which the total precipitable water[1] could at any time be readily determined. It is possible to make an approximate computation of the total precipitable water from radiosonde observations, but this is a time-consuming procedure.

The absorption spectra method employed in the near infrared region of the solar spectrum is, we believe, the most practical means of measuring total precipitable water. The fundamental technique was first described by Fowle (1912). The method with respect to this hygrometer consists of isolating two narrow regions of the solar spectrum: one in a suitable water-vapor absorption band, the other in a nearby region where no absorption occurs. A ratio is established between the irradiance in these two regions. A change of water-vapor concentration in the sensing path changes the ratio. However, when the radiant flux changes due to haze, smoke, mist, etc., the ratio remains essentially unaltered.

---

[1]The term, total precipitable water, is used in accordance with the definition given in the Glossary of Meteorology (1959).

Thus the ratio can be used as an index of the amount of water vapor in the sensing path. The latter quantity can then be divided by the appropriate optical air mass value in order to determine the vertical atmospheric water-vapor content (total precipitable water).

2. Physical concepts

The water-vapor absorption bands are identified with the vibrational and rotational motions of the water-vapor molecules. Ascribed to the three normal modes of vibration of these molecules are three intense bands centered in the infrared near 6.27 μ, 2.77 μ, and 2.66 μ. The last two of these overlap considerably, thereby forming a broad region of absorption that is often referred to in the singular as the 2.7-μ band. A number of other bands, representing various multiples and combinations of the fundamental frequencies, occupy spectral positions from 3.17 μ to 0.57 μ. The more prominent bands of this group are centered in the near infrared at approximately 1.88 μ, 1.38 μ, 1.14 μ, and 0.93 μ (see Fig. 1). A detailed identification of the vibrational components of the water-vapor spectrum can be found in a paper written by Adel and Lampland (1938). Molecular rotation also contributes to the formation of

the bands described above. In a sense, rotational motions serve to shape these bands around the central wavelengths provided by the vibrational motions. Also contained in the water-vapor spectrum is the strong and extensive band that lies in the far infrared beyond the so-called 10-μ window; this band is attributed solely to the effects of rotation. To conclude this brief description of the water-vapor spectrum it seems appropriate to note that the bands diminish in strength more-or-less gradually toward the shorter wavelengths, with those in the visible region exhibiting relatively little absorption.

Care should be exercised in the selection of a band for use in measuring water vapor. A band should be chosen with an intermediate range of fractional absorption for the amount of water vapor likely to be contained in the sensing path. If the absorption is too strong, total absorption may occur when the water-vapor content is high. If the absorption is too weak, the instrument will suffer in sensitivity and instrumental errors will tend to mask true values. The central region of the 0.93-μ band gives a satisfactory range of fractional absorption for the amount of water vapor usually encountered in the path of normal incidence to the sun through the earth's atmosphere (Foster

and Foskett, 1945). A nearby region in the vicinity of 0.88 μ exhibits little or no absorption and therefore serves as an excellent region of reference.

In a spectral region of continuous absorption the relationship between the absorption and the absorbing mass can be expressed as a simple exponential function. However, such a function does not accurately describe the absorption that occurs in the water-vapor bands, since these are not of a continuous character. Actually these bands consist of numerous closely-spaced lines; moreover, the line patterns are irregular in spacing and intensity. The absorption that occurs in a band having such irregularities is actually a complicated process not precisely describable by a simple mathematical formula. Nevertheless, a relationship between the absorption and the absorbing mass does exist, and the curve approximating this relationship in a particular band, or subinterval thereof, can be established by empirical means. Furthermore, in most cases a relatively simple square-root expression closely describes this curve through a limited range of the fractional absorption.

Elsasser (1937, 1938, 1942, 1960) formalized the square-root absorption law, which relates specifically to

subintervals within the infrared water-vapor bands. The square-root law states that the fractional absorption A which occurs in an atmospheric layer of finite thickness is directly proportional to the square root of the absorbing mass X and the square root of the atmospheric pressure P, and inversely proportional to the fourth root of the absolute temperature T. If isobaric and isothermal conditions prevail throughout the layer, then the equation

$$A = K(XP)^{1/2}T^{-1/4} \qquad (1)$$

can be used as an expression of the square-root law. In this equation the factor K is a dimensional constant that depends on the units in which the variables are expressed as well as the spectral characteristics of the particular subinterval under consideration. Elsasser demonstrated that the square-root law closely describes the actual absorption curve in the range of relatively small to intermediate values of the fractional absorption. The reader is directed to the references cited above for further information concerning the limitations of the square-root law as well as for details pertaining to its formulation.

The equation presented above clearly indicates that the absorption spectra method, as it is implemented in this scheme of measuring total precipitable water, is

marked by a degree of uncertainty due to the dependence of the absorption process on the pressures and temperatures through which the atmospheric water vapor is distributed. The approximate mean effects of the distributional relationships are obviously incorporated into the empirical calibration of the spectral hygrometer when radisonde observations provide the comparative data for calibration. We are therefore basically concerned only with the relative errors arising from distributional variations. These errors are briefly discussed in the following paragraphs.

A simple consideration based on Eq (1) shows that the absorption process is relatively insensitive to temperature in the range of temperatures through which the bulk of the atmospheric water vapor is distributed. This temperature range is small in an absolute sense, and the distributional profiles within this range are not excessively variant. Since the absorption varies only as the reciprocal of the fourth root of the absolute temperature, it becomes apparent that the relative errors introduced by the temperature effect are virtually insignificant.

A somewhat similar consideration, based on the same equation, shows that the pressure effect is not prohibitive. The bulk of the atmospheric water vapor normally appears

in the lower troposphere. In other words, the vertical distributions of water vapor are weighted toward the higher pressures. Obviously, the absorption process is relatively less affected by incremental pressure variations at these pressures than at the lower atmospheric pressures. Soundings show that the vertical profiles of atmospheric water-vapor distribution are not excessively variant. In most cases, therefore, the pressure effect does not introduce serious relative errors in this method of measuring total precipitable water.

Howard, Burch, and Williams (1955) observed that the fractional absorption in the entire 0.93-μ band actually varies more nearly as the fourth root, rather than the square root, of the atmospheric pressure. The weaker pressure dependence in the observed case is attributed to overlapping of neighboring spectral lines. The spacing and intensity of the spectral lines—and hence, also the degree of overlapping—are variable in the water-vapor spectrum. Each wavelength interval has its own characteristic fine structure. With this in mind it seems reasonable to conclude that the pressure dependence of the absorption region of the spectral hygrometer, which monitors only a fraction of the wavelengths in the 0.93-μ band, should

differ from that of the entire band. Theoretical considerations as well as some general experimental evidence given in the above-cited report lead us to believe that the actual pressure dependence of this particular absorption interval falls somewhere between the square-root and fourth-root relationships. Further research is obviously needed in this respect.

In their report, Howard, Burch, and Williams (1955) suggest that the actual effect of temperature might also be smaller than indicated in the formal relationship represented by Eq (1). They note that overlapping of neighboring spectral lines should be affected not only by pressure, but also by temperature, since both of these variables appear in the theoretical expression for the width of a spectral line. Thus the argument for ignoring the temperature effect gains even more support. At this point it seems appropriate to note that the slight uncertainties due to the temperature effect should merely serve to partially offset those due to the pressure effect. Considering that temperature as well as pressure decreases with altitude in normal atmospheric profiles, Eq (1) clearly shows that the absorption is oppositely affected by pressure and temperature when a vertical displacement of water vapor occurs.

In view of the foregoing discussions it appears that an empirical calibration of the spectral hygrometer should follow closely, through a limited range of fractional absorption, the simple equation

$$A = K'X^{1/2}. \qquad (2)$$

In this equation the new constant K' incorporates factors representing the integrated mean effects of temperature and pressure as well as the factors ascribed to the constant K in Eq (1).

Thus far we have shown that the absorption spectra method can be expected to give fairly accurate relative measurements of total precipitable water. However, the dependence of absorption on pressure (and to a lesser degree, on temperature) implies that due consideration must be given to certain restrictions inherent to the application of this method:

a. The spectral hygrometer should be operated at elevations close to that of the location where it is calibrated.

b. Use of the instrument should be limited to a reasonable range of optical air mass values.

Obviously, the first restriction is relatively important. King and Parry (1963) describe an actual case,

involving an experimental model of this instrument, which verifies this point. Independent calibrations for this instrument were obtained at two different elevations. A significant difference was observed between the two calibration curves, and an interesting relationship was found between the two curves. More research in this respect is highly desirable in order to determine whether an empirical relationship of this type is adaptable for general applications.

The second restriction is not operationally significant. Basically, it involves the question of whether the uncertainties due to the pressure effect are enhanced at any given fractional absorption when the latter is permitted to occur as a result of widely varying quantities of vertical water-vapor content. A preliminary study, involving vertical atmospheric profiles (water-vapor concentration versus pressure), shows that the variability in the slant-path profiles is not appreciably greater when these profiles result from a wide range of values of vertical water-vapor content compared to a relatively narrow range. Indirect evidence resulting from the empirical calibration procedure and experimental use of the spectral hygrometer also indicates that the uncertainties due to the pressure effect are not

selectively magnified by optical air mass variability.

The discussion in the foregoing paragraph does not take into account the inherent uncertainties attending very low solar elevation angles. These uncertainties are primarily related to the effects of refraction and excessive scattering, and to possible timing errors associated with the rapidly-changing long optical paths.

3. Description of the instrument

The optical components. The two spectral regions of interest are isolated by first-order, narrow-band-pass interference filters. The filters are placed in the box housing in front of the photocells (see Fig. 2). In operation the solar beam remains at normal incidence to the filters since the hygrometer is continuously aimed at the sun. The following data summarize the normal-incidence characteristics of these filters: The filter that isolates the region of absorption has its central wavelength at 0.935 μ, a peak transmittance of 43%, and a half-width of 13 mμ; the filter used for isolating the reference region has its central wavelength at 0.881 μ, a peak transmittance of 50%, and a half-width of 13 mμ. $\simeq 130$ Å

Parallel tubes of 12-in. length and 1 7/8-in. i.d. are used for collimating the sunlight. Sharp-cutoff red filters, Corning C.S. No. 2-61 (transmittance <0.5% at wavelengths below 0.590 μ), are installed at the forward ends of the collimating tubes to provide protection from the weather as well as to prevent the transmission of radiation through possible passbands of higher order. In order to minimize errors due to internal reflections, a diaphragm with 1 3/8-in. i.d. is flush-mounted in the front end of each tube immediately behind the cutoff filter. A Plexiglas window is installed behind the collimating tube assembly, thereby isolating the box-housing chamber for more efficient thermostating of the photocells.

The photocells. Silicon solar cells with 1-in.-diam active surfaces are used as the radiation detectors. They are very fast in response ($\lesssim$20 μsec), and have exceptionally stable, long-life performance characteristics. A properly matched pair of these cells gives continuous ratios of the photocurrents in direct proportion to the ratios of the in-band to out-of-band solar energies. Laboratory tests verified the reliability of these cells.

Silicon solar cells exhibit a relatively high current response in the near infrared region at which this hygrometer

operates. The spectral response range of this type of photocell extends approximately from 0.35 μ to 1.15 μ, with a maximum response occurring near 0.75 μ. The photocells used have a nominal efficiency of about 10% in the region of maximum response.

The response of these cells to incident light energy was found to be somewhat dependent on the ambient temperature. Temperature stability was achieved by thermostating the photocell mounting block at 100°F. This operating temperature also serves to prevent condensation from forming on the internal optical surfaces.

The current output of a silicon solar cell is directly proportional to the intensity of light incident upon its active surface when the load across the cell is small, approaching short circuit. Laboratory experiments were conducted to test the cells for linearity under increased external loads. The levels of illumination were adjusted so that the range of output current of each photocell was comparable to the range that it generates during normal operation of the spectral hygrometer. The results of these experiments indicate that under the simulated conditions of effective illumination the output current of this type of photocell begins to fall off very slightly from linearity as the external resistance is increased to

values above about 10 ohms. This deviation was found to be relatively small even for resistances as high as 50 ohms. The deviation then increased more sharply for higher resistances. Although tests showed the nonlinearity to vary with different cells, it was found that by proper selection pairs could be matched for similar deviations. By installing a pair of matched photocells in the hygrometer and keeping the external resistances fixed at specific values less than 50 ohms, it was possible to obtain ratios of output current proportional to the ratios of incident radiant energy. The error in the obtained ratios was always less than 1/2% regardless of the overall intensity of the incident beam.

Fluctuations in the overall intensity of the incident solar beam are related primarily to the processes of scattering and diffuse reflection by the atmospheric constituents. The effect of the gaseous constituents is slight, and that of the nongaseous constituents such as smoke, dust, and haze is somewhat greater. But obviously the greatest effect is that of clouds. However, these light-attenuating mechanisms are essentially nonselective in the near infrared region within which the hygrometer operates. Therefore, since the hygrometer gives a linear ratio response with properly selected values for the fixed external resistances across the

photocells, the ratio given by the hygrometer represents primarily a measure of the water vapor contained in the atmospheric sensing path regardless of the fluctuations in the overall intensity of the incident beam.

The foregoing statement is true only as long as the incident sunlight is sufficiently intense for the photocells to provide the minimum current necessary for the self-balancing ratio bridge[2] to find a balance point. In practice, when thin clouds appear in the path of the solar beam, a balance will occur only while the sun continues to cast relatively discernible shadows. In this case, the direct-beam intensity corresponds roughly to about 15% of that obtained with full sunlight. Below this level of illumination the response of the recorder fails rapidly, and the scale error increases quite sharply. Future experimentation may show that increased amplification will permit this hygrometer to give valid readings even though the sunlight is obstructed by denser clouds.

The equatorial mounting. In order to get a continuous record of water-vapor measurements, the hygrometer is placed

---

[2]This circuit employes a conventional potentiometric recorder which has been modified for use as a ratio bridge.

on a motor-driven equatorial mounting (see Fig. 3) and trained on the sun. The mounting (also developed by the Weather Bureau) is weather-tight and capable of following the sun throughout the day without attention.

The ratio-bridge circuit. A schematic diagram of the self-balancing ratio-bridge circuit is shown in Fig. 4. The two photocurrents are fed into the bridge circuit. The ratio of the photocurrents is registered directly on the recorder chart. The following discussion with reference to Fig. 4 explains the relationship of the photocurrents to the recorded ratios.

Several considerations led to the arbitrary choice of 40.0 ohms for R_a and 20.0 ohms for R_s. Among the factors considered were ratio-bridge sensitivity, recorder resolution, standardization of the recorder readings to the hygrometer ratios, and linearity of hygrometer ratios (see discussion on photocells). Further laboratory tests of this hygrometer indicated that the linearity consideration requires a total of 36.0 ohms across the reference-band photocell when 40.0 ohms are placed across the absorption-band photocell. Consequently, the sum of R_b and R_t must be held constant at 16.0 ohms.

When a balance of the bridge occurs, the potential drop in one arm of the bridge equals that in the other. This is expressed by the equation $I_a R_a = I_r R_r$, from which we obtain the useful relationship $I_a/I_r = R_r/R_a$. The latter equation states that the ratio of the photocurrents varies inversely as the ratio of the resistances which are effective in the balancing process. This ratio of effective resistances is a direct function of the balance position of the bridge. Therefore the recorder gives a direct reading of the desired ratio of the photocurrents.

An example, in accordance with the designations in Fig. 4, clarifies the above relationship. As previously noted, R_a and R_s are fixed respectively at 40.0 ohms and 20.0 ohms. Assume in this case that R_b is set at zero and R_t at 16.0 ohms. (R_t is in the photocell loop, but never becomes part of the bridge circuit.) Now, if the recorder balances at half scale, R_e is 10.0 ohms and the ratio becomes $I_a/I_r = R_r/R_a = (R_b + R_e)/R_a = (0 + 10.0)/40.0 = .250$. Obviously these resistance values establish a ratio span of .000 to .500 across the recorder.

The hygrometer herein described normally operates in a range of ratios from .200 to .700, except with low solar elevations in very humid weather (see Fig. 5). The equation

in the paragraph above reveals that the ratio span of the recorder is shifted to match the usual range of hygrometer ratios (.200 - .700) by simply setting R_b at 8 ohms. (R_t is then also set at 8 ohms.) In practice, R_b and R_t can be designed into the circuit so that corresponding increments (e.g., 4-ohm steps) can be simultaneously added and subtracted (or vice versa) by means of a 2-pole rotary selector switch. This step-resistance arrangement also facilitates the use of the recorder with any of several spectral hygrometers.[3]

4. Calibration

The calibration procedure consists of comparing the hygrometer ratios as shown by the recorder against the corresponding quantities of water vapor that exist in the respective sensing paths at the times of these comparisons. Usually the

---

[3]The ratio range of a particular hygrometer depends primarily on the combined effects of the respective characteristics of the narrow-band-pass filters, the corresponding responses of the photocells, the relative solar intensities in the respective wavelength intervals, and the fractional absorption coefficient for the specific wavelength interval of the absorption passband.

amount of water vapor in the sensing path is expressed in inches (or centimeters) of precipitable water. Experience shows that no simple method of calibration is available. A calibration using laboratory facilities is not feasible because of the excessive path lengths required to duplicate the typical quantities of water vapor that exist in the atmospheric paths of the solar beam. Furthermore, laboratory techniques can only yield constant-pressure calibration data. Since theoretical and experimental knowledge regarding the pressure effect is still somewhat limited, adjustment of these data in an attempt to approximate average conditions prevailing in the solar-inclined atmospheric paths would, at this time, only add further complications and uncertainties. The decision was therefore made to obtain an approximate empirical calibration which makes use of radiosonde measurements.

The spectral hygrometer measures the amount of water vapor X in the atmospheric path of the solar beam, whereas the radiosonde measurement represents the approximate amount of water vapor W in a vertical column of the atmosphere. The calibration procedure therefore requires that the quantity determined from the radiosonde data must in each case be multiplied by a proportionality factor: the ratio of the length of the solar-inclined atmospheric path to that of the

zenith atmospheric path. This ratio m, the optical air mass, is approximated by csc α, where α is the elevation angle of the sun. The optical air mass is expressed more precisely by Bemporad's formula[4], particularly for solar elevations below 20°. The solar elevation angle can be obtained from appropriate tables or curves, or it can be measured directly at the time of observation; the method used in determining this angle depends largely on the facilities available and the number and frequency of the desired observations.

The tentative calibration shown in Fig. 5 consists of a plot of the recorded hygrometer ratios R versus appropriate optical air mass multiples mW of the corresponding radiosonde evaluations of total precipitable water. All plotted points in this calibration were obtained from simultaneous observations taken at the Observational Test and Development Center[5], U. S. Weather Bureau, Washington, D. C., on favorable days from June, 1961 through April, 1962. A more precise calibration of this hygrometer is now being pursued.

---

[4]Bemporad's formula together with computations in terms of z, the complement of α, can be found in Table 137 of Smithsonian Meteorological Tables, 6th rev. ed. (1951).

[5]Lat $38^{\circ}59'$N, long $77^{\circ}28'$W, elev 276 ft MSL.

5. Concluding remarks and discussions

Instrumental reliability. The following general statements are presented concerning the reliability of the spectral hygrometer:

a. Laboratory tests have proved the stability and linearity of the instrumental equipment. These tests showed that the accuracy of the hygrometer is not degraded by ambient temperature variations or by intensity fluctuation of the incident radiation.

b. Experimental operation has provided strong evidence of the dependability and relative accuracy of the instrument. Changes in total precipitable water as detected by the spectral hygrometer were quite consistently comparable to those changes indicated by successive radiosonde measurements, regardless of the altitude, and hence pressure, at which the changes occurred. Further confidence was established by means of another spectral hygrometer of the same design. The second instrument was operated simultaneously on an adjacent mounting during the calibration period. The records from the two instruments

showed a striking agreement in relative measurements by consistently indicating identical changes in total precipitable water over both short and long periods of time.

c. A preliminary study of an approximate nature was recently made in an effort to obtain a numerical appraisal of the pressure effect. The associated computations involved variations in the vertical distributional profiles of water vapor as shown in roughly 150 radiosonde records obtained during the calibration period. Results of this study indicate that the pressure-induced uncertainties in this method of measuring total precipitable water should normally not exceed .03 to .05 inch. Extreme variations in the vertical profiles might cause occasional errors up to .10 inch. Further studies of this type together with more thorough knowledge regarding the pressure effect are required before a more definite statement can be made in this respect.

Possible applications. The availability of continuous measurements of total precipitable water suggests several distinct uses for the spectral hygrometer. Local correlation studies between total precipitable water and

other meteorological variables become more feasible. These studies might include such factors as atmospheric stability, probability of precipitation or thunderstorms, amount of precipitation, or minimum temperature. An important application might be in the field of agricultural meteorology, especially with respect to the prediction of damaging frost. A suitable network of spectral hygrometers could provide important information regarding the movement and extent of moist tongues, which are of particular interest to the forecasters of severe weather. This type of network may also prove useful in conservation activities, particularly in the field of applied hydrology. Research in the realm of physical meteorology may offer further possibilities of instrumental application.

Acknowledgments. The authors wish to express their appreciation to Messrs. Elbert W. Atkins and Theodore Walters of the Observational Test and Development Center for providing technical assistance and facilities relevant to obtaining and analyzing the radiosonde data, to Dr. Earle K. Plyler of the National Bureau of Standards for his authoritative advice pertaining to water-vapor absorption bands, and to Mr. Ralph Stair of the National Bureau of Standards for providing spectrophotometric analyses of the narrow-band-pass filters.

REFERENCES

Adel, A., and C.O. Lampland. "A new band in the absorption spectrum of the earth's atmosphere." Astrophys. J. 87, 198-203 (1938).

Elsasser, W. M. "On some properties of the water-vapor spectrum and their relations to atmospheric radiation." Mon. Wea. Rev. 65, 323-326 (1937).

———. "New values for the infrared absorption coefficient of atmospheric water vapor." Mon. Wea. Rev. 66, 175-178 (1938).

———. "Heat transfer by infrared radiation in the atmosphere." Harvard Meteorological Studies No. 6, 107 pp. (1942).

———, with M. F. Culbertson. "Atmospheric radiation tables." Meteorological Monographs 4, No. 23, 43 pp. (1960).

Foster, N. B., and L. W. Foskett. "A spectrophotometer for the determination of the water vapor in a vertical column of the atmosphere." J. Opt. Soc. Am. 35, 601-610 (1945).

Fowle, F. E. "The spectroscopic determination of aqueous vapor." Astrophys. J. 35, 149-162 (1912).

Howard, J. N., D. E. Burch, and D. Williams. "Near-infrared transmission through synthetic atmospheres." Geophysical Research Papers No. 40, 244 pp. (1955).

Huschke, R. E. (editor). Glossary of Meteorology. American Meteorological Society, Boston, p. 437 (1959).

King, R. L., and H. D. Parry. "Field tests and calibration of the total atmospheric water-vapor hygrometer." Paper presented at the 1963 International Symposium on Humidity and Moisture, Washington, D. C., May, 1963.

List, R. J. (editor). Smithsonian Meteorological Tables, 6th rev. ed. Smithsonian Institution, Washington, D. C., p. 422 (1951).

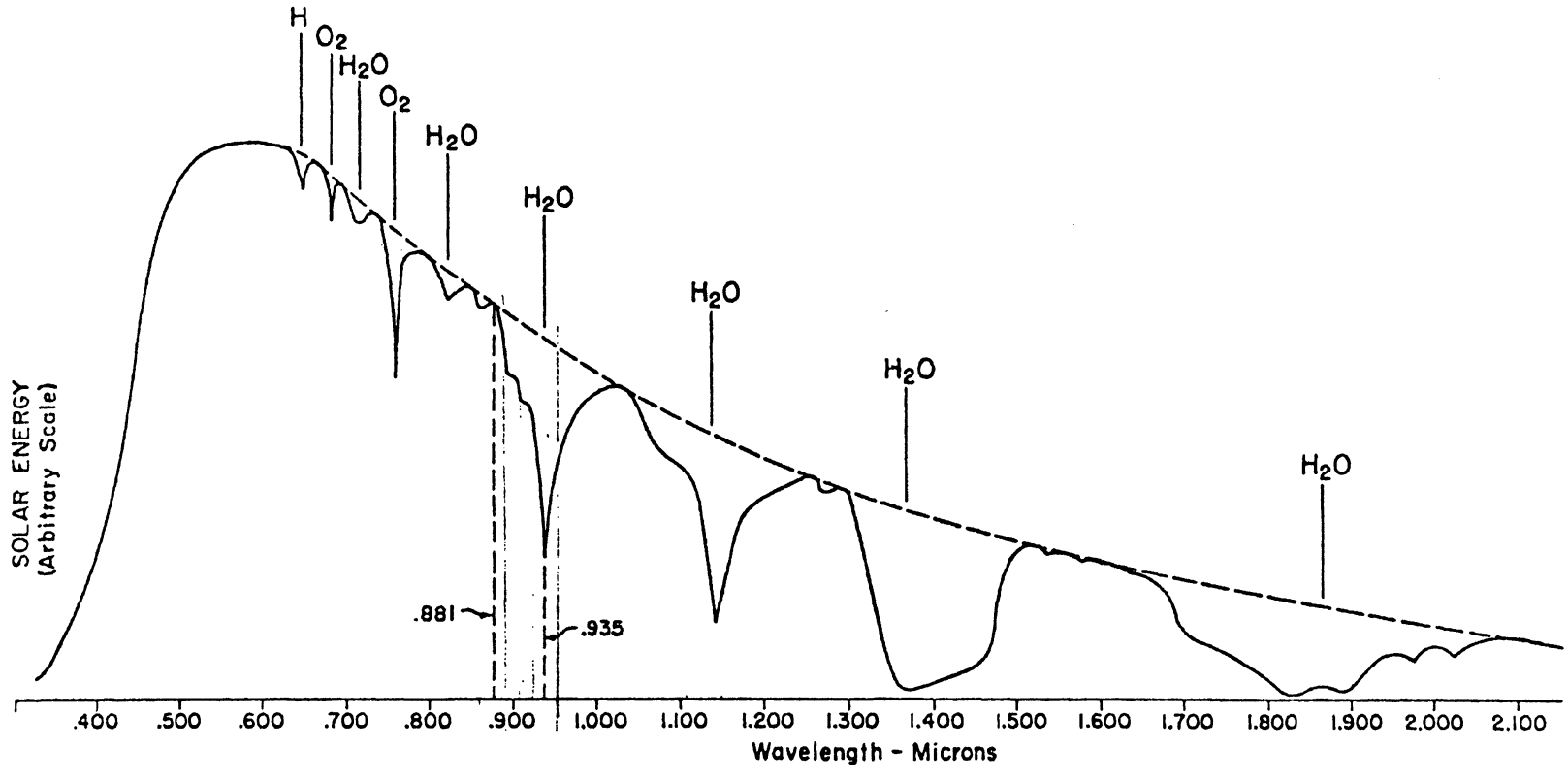

Fig. 1. Curve showing the approximate solar energy distribution at sea level through the visible and part of the near-infrared regions. Notation is made of the reference and absorption band centers. Some of the more prominent bands of absorption are indicated. Ordinates are in arbitrary units, not strictly to scale.

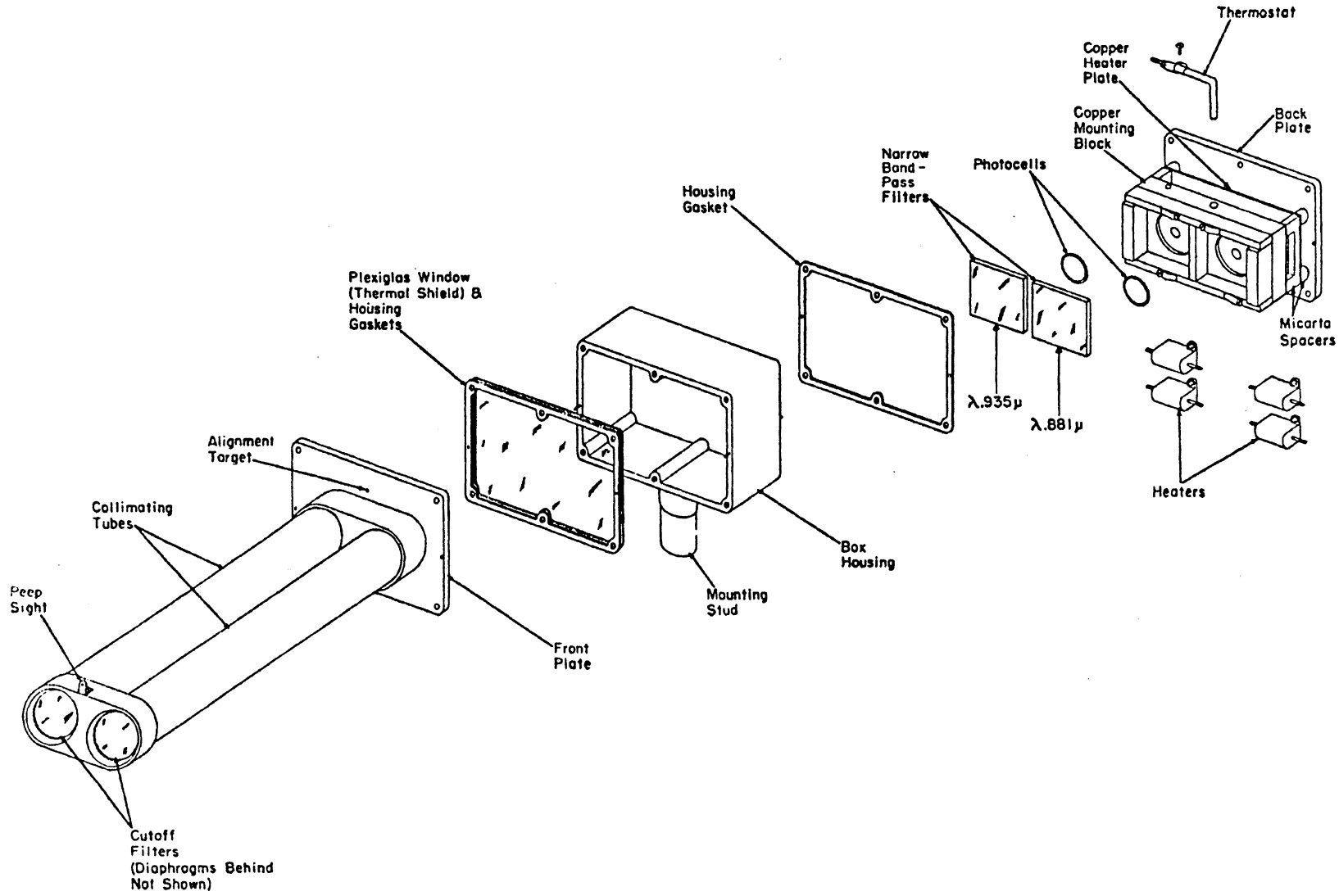

Fig. 2. Exploded view of the spectral hygrometer showing the relative orientation of the various components.

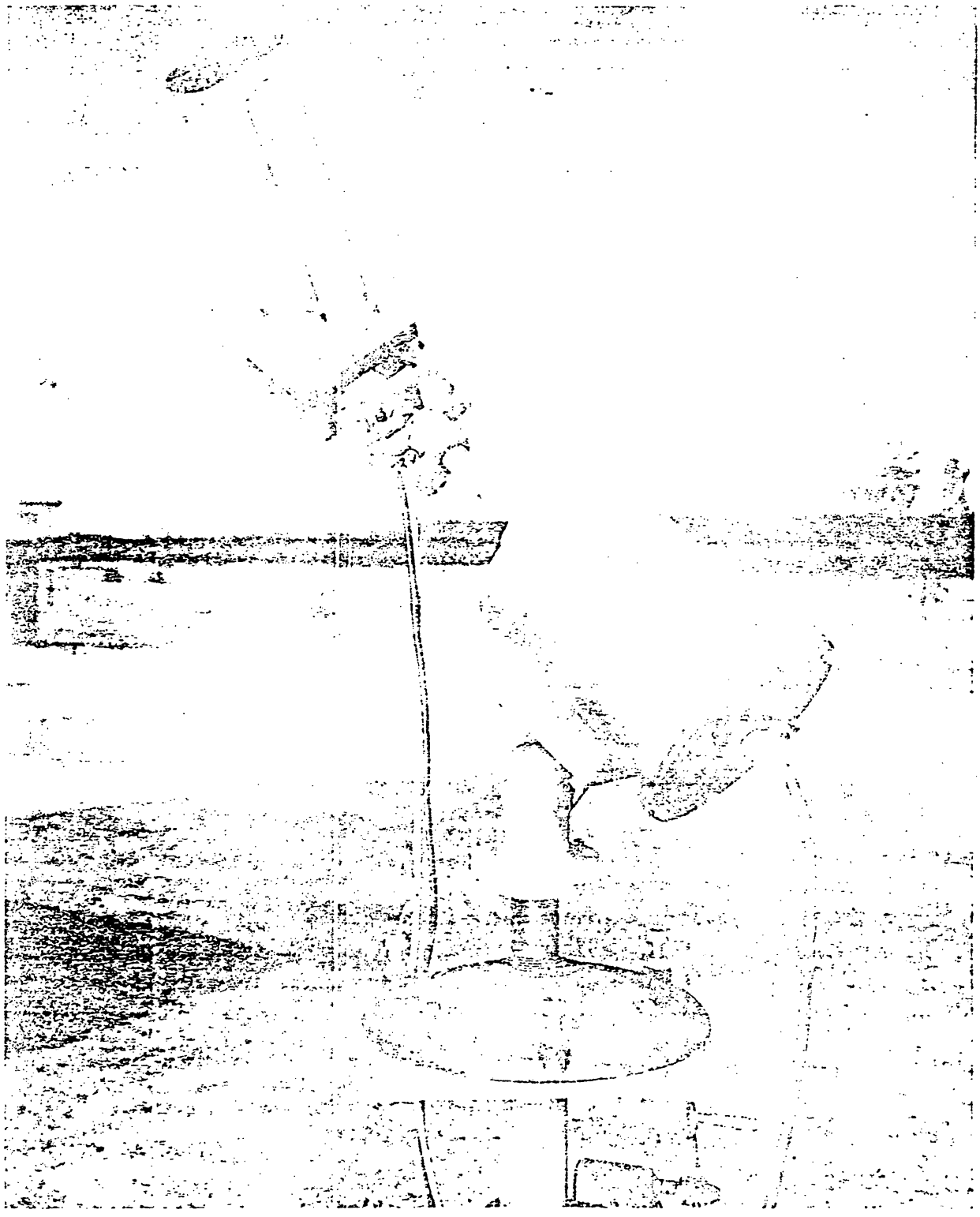

Fig. 3. Spectral hygrometer on an all-weather, solar-tracking equatorial mounting.

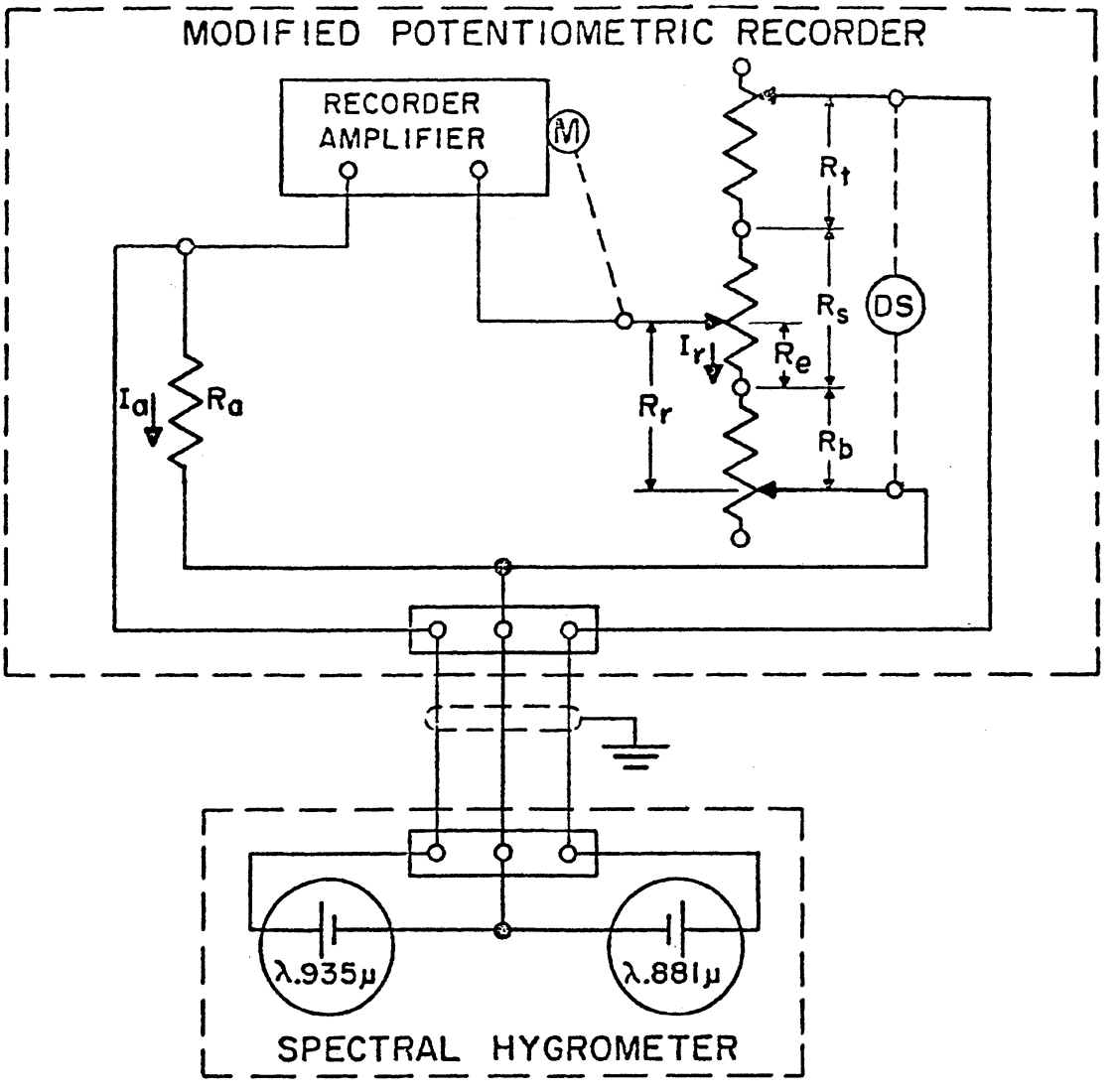

Fig. 4. Schematic diagram of the ratio-bridge circuit. I_a--current from the absorption-band photocell; I_r--current from the reference-band photocell; R_a--40.0 ohms, the total resistance across the absorption-band photocell, which is also across the input of the recorder; $R_r = R_b + R_e$--the part of the resistance in the reference loop that is effective in the ratio bridge (i.e., the total resistance below the balance point); R_s--20.0 ohms, the entire resistance of the slidewire; R_e--the part of the slidewire resistance below the balance point; R_b--zero suppression resistance, or the variable resistance below the slidewire which is used for shifting the ratio range of the recorder to match the operational ratio range of the hygrometer; R_t--compensating resistance, or the resistance above the slidewire which is varied simultaneously with R_b so that the external resistance across the photocell remains constant; DS--the 2-pole rotary selector switch which facilitates the simultaneous changing of R_b and R_t in equal amounts; M--the balancing motor.

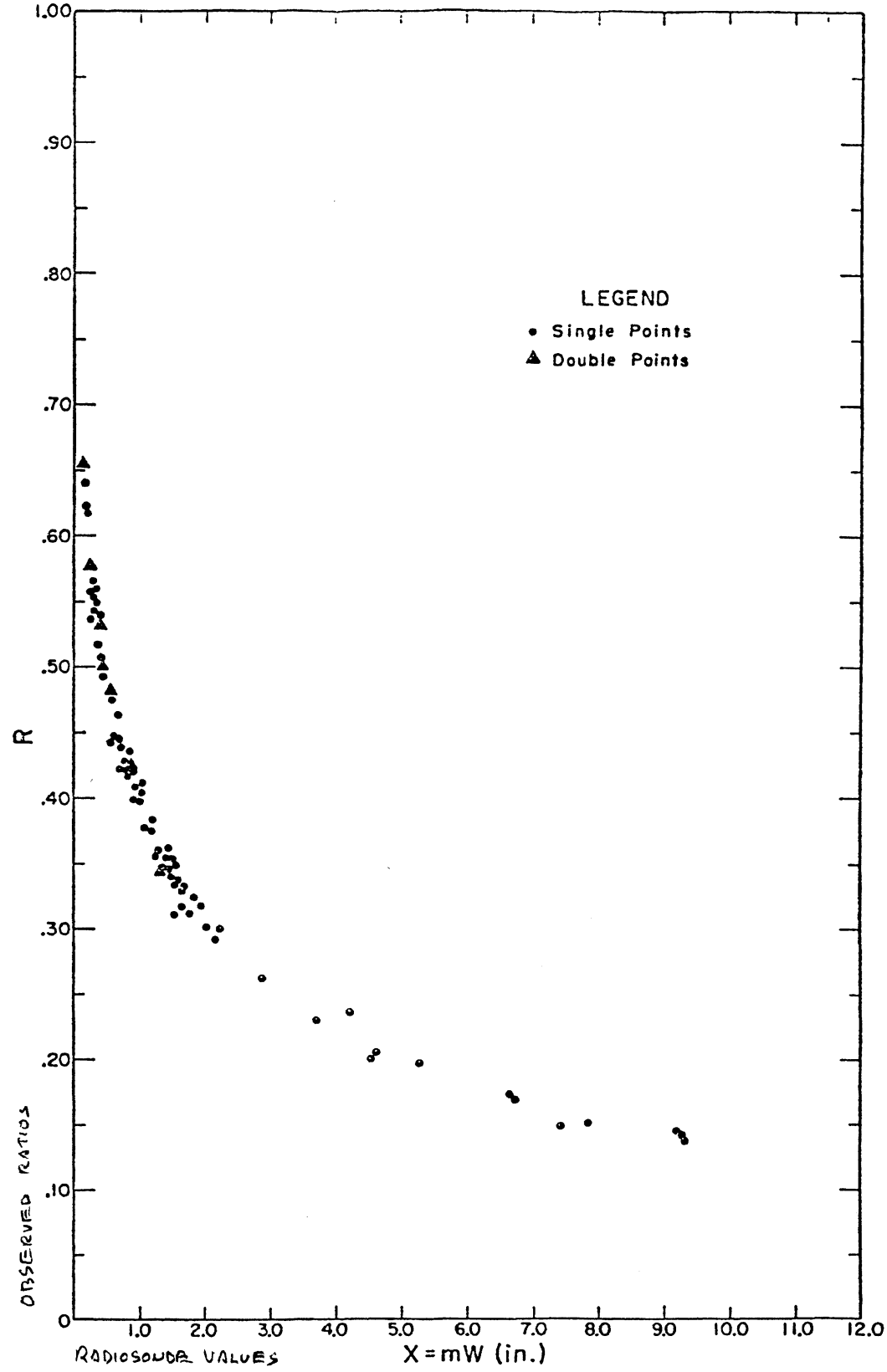

Fig. 5. The tentative calibration of the spectral hygrometer. The curve represented by the plotted points gives the mass of water vapor X in the sensing path as a function of the hygrometer ratio R. The total precipitable water can be readily determined by means of the equality $W = X/m$, where m represents the optical air mass at the time of observation.

NATIONAL RADIO ASTRONOMY OBSERVATORY
Green Bank, West Virginia

Millimeter Wave Internal Report

A COMPARISON OF MEAN PRECIPITABLE WATER-VAPOR AT SEVERAL SELECTED LOCATIONS USING AN IMPROVED TYPE WATER-VAPOR HYGROMETER

Frank J. Low

DECEMBER 1964

NUMBER OF COPIES: 30

THE NRAO PRECIPITABLE WATER SURVEY

During the past year the NRAO has developed and calibrated a number of portable spectral hygrometers for measuring total atmospheric water vapor. In addition to measurements made at Green Bank and at selected sites by NRAO personnel, we have been fortunate to receive data from the High Altitude Observatory, the University of Arizona, and Kitt Peak National Observatory. All of the instruments have been intercompared and the compiled data have been reduced to unit air mass. These data are given in tabular and graphical form.

It is anticipated that more data will be collected in the future and a recompilation will be made when necessary. The appendix describes the instrument, its use and calibration.

SITE DESCRIPTION

Green Bank, West Virginia

Located 180 miles west of Washington, D. C. at an elevation of 2690 ft.; site of National Radio Astronomy Observatory.

Kitt Peak, Arizona

Located 45 miles southwest of Tucson, Arizona, at an elevation of 6760 ft. Readings taken at the Solar Telescope of the Kitt Peak National Observatory.

Catalina Mountains, Arizona

Optical observing site of the University of Arizona, approximately 35 miles northeast of Tucson, Arizona at an elevation of 8300 ft.

Climax, Colorado

Seventy miles southwest of Denver at 11,150 ft.; the site of the High Altitude Observing Station.

Mt. Pinos, California

Located 60 miles northwest of Los Angeles; 8830 ft.

Jet Propulsion Lab, Pasadena, California

Elevation 770 ft.

Table Mountain, California

50 miles northeast of Los Angeles; 7500 ft. in height.

DISTRIBUTION OF HYGROMETERS

Hygrometer	Designation
*A(3-1)	Used by NRAO observers until July 1964 when it was taken to Kitt Peak.
A(1-3)	Sent to John Firor at Boulder, Colorado (3/16/64).
A(4-2)	At Climax, Colorado.
A(2-4)	Shipped 3/12/64 to Harold Johnson, Tucson, Arizona.
B(3-3)	Mailed to Bruce Gary, Jet Propulsion Lab, on 2/18/64.
B(4-4)	Currently in use at NRAO
B(1-1)	With Gerald Kuiper at University of Arizona
B(2-2)	Spare in Lab at NRAO

*A calibration curve is included for this hygrometer.

COMPARISON COMPILATION $\frac{mm}{AM}$ (Cont.)

Month	Day	Green Bank	Climax	Kitt Peak	Catalina	Table Mtn.	Mt. Pinos	JPL
March	19	2.99						
	20		0.97					
	23	3.25						
	24	6.68						
	27	2.04			1.6			
	28				2.1			
	29		1.51					
	30		1.73		2.24			
April	1		3.86					
	2				2.40			
	7				1.33			
	8				1.33			
	9	6.53			1.29			
	10	4.41			1.70			
	11	3.09	1.82					
	12		1.49					
	13				1.50			
	14		2.02		1.40			
	15		1.94		2.20			
	16	6.11	2.13		2.00			
	17	5.51			2.95			
	18				3.2			
	20				2.1			
	21				1.4			
	25	3.00			2.1			
	26				1.8			
	29		2.48					
May	1	4.00						
	4	7.37						
	5	7.18						
	6	8.14						
	7				2.25			
	9				1.3			
	10				3.3			
	11	10.60						
	12				2.82			
	15	4.84	2.47					
	16	4.78						
	17				3.14			
	18	7.66						
	19	11.70						
	20	7.73						
	21	6.65						
	22	9.47			4.19			
	24		4.3					
	25	4.58						
	26	7.85						

COMPARISON COMPILATION $\frac{mm}{AM}$ (Cont.)

Month	Day	Green Bank	Climax	Kitt Peak	Catalina	Table Mtn.	Mt. Pinos	JPL
May	28		2.88					
	29				1.93			
June	1				3.65			
	2				3.44			
	4	6.95						
	5	8.10						
	6				4.18			
	8				3.61			
	9		2.47		4.65			
	10		2.44		3.27			
	11	7.30	1.95					
	12	12.80	2.03		4.0			
	13				3.59			
	14				4.36			
—	15		4.86		1.82			
	16	7.0			3.81			
	17	9.1			5.6			
	18				4.28			
	19		2.16		3.81			
	20		2.93					
	21		3.21		2.95			
	22				3.04			
	23		2.61		4.0			
	24		3.52					
	25	8.2	3.50		3.33			
	27		5.8					
	28		5.53					
	29	13.8						
	30		4.28					
July	1		3.74					
	5		6.62					
	6		5.50		6.14			
	7	12.8						
	8		4.08					
	9		4.81					
	10		7.76					
	11		3.40					
	15		6.71					
	16		8.46					
	17				12.0			
	18		6.60					
	22		7.59					
	25		3.67					
	26		2.41					
	28	23.5		10.2	11.5			

COMPARISON COMPILATION $\frac{mm}{AM}$ (Cont.)

Month	Day	Green Bank	Climax	Kitt Peak	Catalina	Table Mtn.	Mt. Pinos	JPL
Oct.	23				5.07			
	24			2.83				
	25			3.12				
	26	7.13						
	27	4.83						
	30	7.22						
	31			1.91				
Nov.	1	8.25						
	2	7.55			2.13			
	4	6.85		2.15	1.71			
	6	5.30						
	9	5.72						
	11			1.89				
	12			1.66				
	13	5.4		1.69				
	16				0.83			
	17	6.35		0.88	1.20			
	20	3.27		0.61				
	21			0.57	0.76			
	22	3.23		0.88				
	23	2.98		1.95	1.83			
	24				1.50			
	25				2.37			
	28			2.07				
	29			2.16				
	30			1.71				
Dec.	1	3.08						

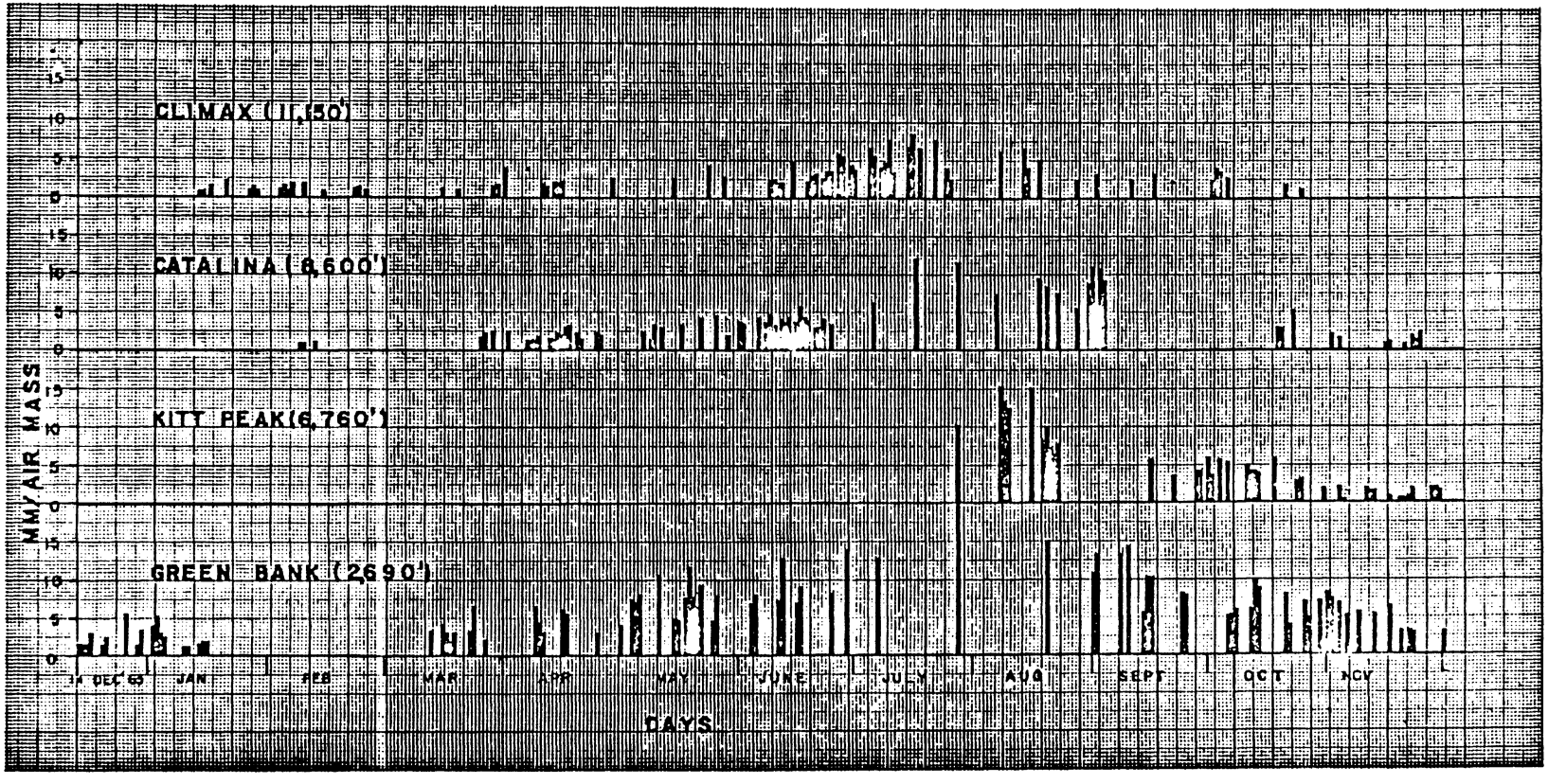
CLIMAX (11,150')
CATALINA (8,600')
KITT PEAK (6,760')
GREEN BANK (2690')
MW AIR MASS
15
10
5
0
14 DEC 63
JAN
FEB
MAR
APR
MAY
JUNE
JULY
AUG
SEPT
OCT
NOV
DAYS

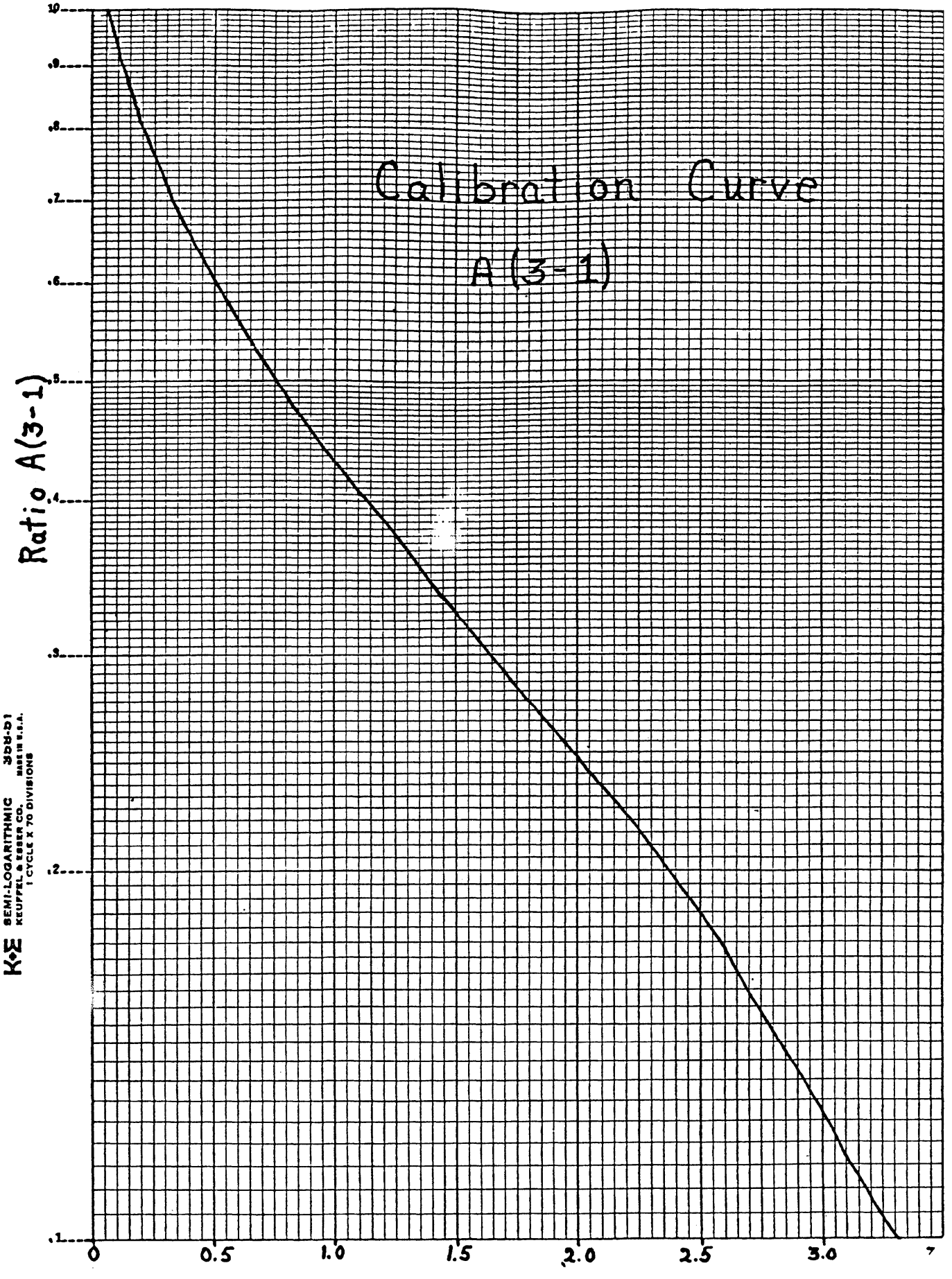
Calibration Curve
A(3-1)
Ratio A(3-1)
10
.9
.8
.7
.6
.5
.4
.3
.2
.1
0
0.5
1.0
1.5
2.0
2.5
3.0
K+E SEMI-LOGARITHMIC 359-51
KEUFFEL & ESSER CO. MADE IN U.S.A.
1 CYCLE X 70 DIVISIONS

APPENDIX - The Portable Spectral Hygrometer

The basic principle is that developed by F. E. Fowle (Ap. J. 35, 149, 1912) and used by N. B. Foster, D. T. Volz and L. W. Foskett in their spectral hygrometer. Our design employs a single silicon diode to drive a resistive but rugged microammeter, thus yielding a highly portable hand held instrument. The spectral characteristics of the diode are the same as the silicon solar cell used in the Weather Bureau's instrument and the two filters are also essentially the same. The diode has excellent linearity and high output. Our calibration does not change noticeably with ambient temperature, and external power is not required. Except for differences in the linearity of the different types of detector, the NRAO instrument has a calibration curve similar to the Weather Bureau's instrument. This is quite helpful because it enables us to calibrate one of our instruments by comparison at the Weather Bureau in Washington with one of Mr. Volz's instruments.

The diagram shows the very simple circuit:

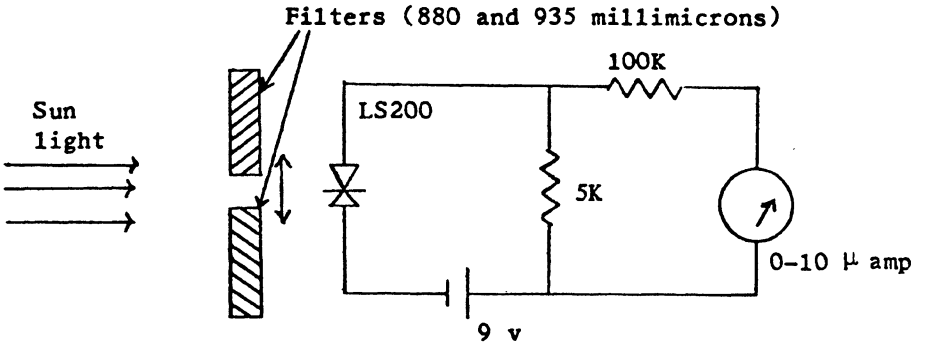

To make a reading the instrument is pointed at the sun with the 880 filter in front of diode. The meter will deflect nearly full scale. The reading should be carefully maximized and noted. With the 935 filter the deflection is somewhat less and depends strongly on the precipitable water vapor in the path. The ratio of the two readings is recorded along with either the time or solar zenith angle. An on-off switch is not required since negligible current flows when no sun light falls on the diode. The calibration curve gives the total water vapor in the path. This number is then reduced to units air-mass by means of the secant z formula.

Hygrometer A 3-1 was calibrated as follows: Fowle's data from absorption tube experiments was used to establish the shape of the curve at low water vapor levels. Comparison with Volz's instrument at higher levels provided an absolute reference since his instrument was empirically calibrated against radio sonde data. In addition A 3-1 was flown in a U-2 aircraft at Lockheed. After correcting on the ground for the effect of the airplane canopy, the reading at high altitude provided the zero point. We are indebted to both Mr. D. T. Volz of the U. S. Weather Bureau and to Lockheed Aircraft for their assistance.